Theoretical analysis of two-body electrodisintegration of ^{3}He

E. van Meijgaard
TRIUMF, 4004 Wesbrook Mall, Vancouver, British Columbia, Canada V6T 2A3

J. A. Tjon
Institute for Theoretical Physics, Princetonplein 5, P.O. Box 80.006, 3508 TA Utrecht, The Netherlands
(Received 18 January 1990)

The theoretical framework of calculating the electron induced two-body breakup reaction ^{3}He$(e,e'p)d$ at intermediate momentum transfer is described, where nucleonic final-state interactions are exactly accounted for. A nonrelativistic dynamical description is assumed and the half-off-shell scattering state wave functions needed for such a calculation are determined by solving the Faddeev equations with Padé approximant technique. Local s-wave spin-dependent potentials are used as two-nucleon input.

I. INTRODUCTION

In the last decade, considerable progress has been made in the single nucleon knockout reaction in inelastic electron scattering.[1] The electron is considered as a powerful probe to study the precise dynamical behavior of nucleons inside the nucleus for two reasons. The electromagnetic interaction is well known and the nuclear structure is only weakly affected by it. With the primary objective to determine the proton momentum distribution inside the three-nucleon system and to study the reaction mechanism, the electron induced breakup reaction of the ^{3}He nucleus into a proton and a deuteron is measured at Saclay[2,3] and at NIKHEF, Amsterdam.[4,5]

In the theoretical analysis it is customary to assume that the active nucleon is directly knocked out, leaving the residual pair in a deuteron state or an unbound, but correlated state. In the plane wave impulse approximation (PWIA), the experimental data fall well below the available theoretical predictions, in which the trinucleon bound state was calculated by a Faddeev[6] or variational[7] technique. This discrepancy is usually ascribed to inadequacies of the bound state wave function. However, in principle the mechanism of direct nucleon knockout is not correct and final-state interactions between the nucleons after the photon is absorbed have to be analyzed before reliable physical information from the breakup experiments can be extracted.

In this work we present an exact analysis of the electromagnetic breakup process of the trinucleon system. Nucleonic final-state interactions (FSI) are fully accounted for by solving the Faddeev equations for the relevant scattering states. The nuclear dynamics are treated nonrelativistically and the nucleon-nucleon interactions are restricted to the s-wave channel. It is stressed that the generally accepted conjecture that the size of final-state effects is small and can be neglected in good approximation at least at low missing momenta has not been confirmed by an explicit theoretical study. Final-state effects have been accounted for in a approximate way by Laget,[8,9] who calculates the coincidence cross section from the first few terms of a diagrammatic expansion of the full transition amplitude. In addition to the FSI corrections Laget also includes meson exchange current (MEC) effects. His results seem to give an adequate description of the data; unfortunately his treatment is not systematic in terms of a conventional nuclear model.

Finally, we like to mention that the first exact three-body calculation was presented by Barbour and Philips,[10] almost two decades ago, in order to account for final-state effects in low energy photodisintegration. Later Lehman *et al.*[11] were the first to calculate the electron induced two-body breakup process including FSI, using a nonrelativistic expression for the nucleon current. In both calculations the Faddeev equations were solved, employing a simple nonrealistic separable potential. The recent accurate $(e,e'p)$ electron scattering data at higher momentum transfer clearly calls for theoretical calculations with more realistic two-nucleon interactions. In our investigations we have used local spin-dependent s-wave NN potentials[12] as input to the three-body equations. They have the attractive property that they give a reasonable description of the elastic and breakup processes in nucleon deuteron scattering[13] in the region up to 100 MeV lab energy.

The outline of this paper is as follows. In Sec. II the one-photon exchange formalism is briefly reviewed. The relevant components of the nuclear current are discussed and the off-shell one-body current matrix elements are derived to accommodate the evaluation of the trinucleon nuclear structure functions. Section III is devoted to some aspects of the three-body dynamics. To facilitate the numerical evaluations the unitary pole expansion (UPE) is employed to describe the local s-wave spin-dependent interaction in a series of separable potential terms. The UPE convergence properties for the trinucleon bound state as well as for the NN and Nd scattering observables are investigated. In view of the electromagnetic two-body breakup analysis the general form of the trinucleon bound state wave function and the half-off-shell wave functions for $3N \rightarrow Nd$ scattering are described. In Sec. IV the nuclear structure functions of the

electromagnetic two-body breakup process are derived and exactly calculated.

II. ELECTROMAGNETIC INTERACTION

In this section we briefly recall the general form of the cross section for the unpolarized $A(e,e'p)A-1$ reaction. In order to calculate the electromagnetic amplitude of the transition from a trinucleon bound state to a *Nd* final state, which are both eigenstates of the full three-particle Hamiltonian, we assume the nuclear current to be composed of one-nucleon currents only. All arguments presented are only valid in the intermediate energy domain. The incident electron energy is typically of the order of 500 MeV. The momentum transfer varies from 200 MeV/c to 600 MeV/c, while the energy transfer in the lab system is generally smaller than 200 MeV, below the threshold of pion production.

A. One-phonon-exchange formalism

Since the electromagnetic interaction is relatively weak, the scattering of an electron from a nucleus can very well be described by the exchange of one photon, which transfers energy and momentum to the nuclear system. Schematically the one-photon-exchange model can be represented by Fig. 1. The four-momenta stand for

$(k_e)_\mu=(\mathbf{k}_e;iE_e)$, incoming electron ;

$(k_{e'})_\mu=(\mathbf{k}_{e'};iE_{e'})$, outgoing electron ;

$(q)_\mu=(\mathbf{Q};i\omega)$, transferred photon ;

$(P_A)_\mu=(\mathbf{P}_A;iM_A^*)$, target nucleus ;

$(P_{A-1})_\mu=(\mathbf{P}_{A-1};iM_{A-1}^*)$, residual nuclear system ;

$(p'_N)_\mu=(\mathbf{p}'_N;iE_{p'_N})$, detected nucleon .

Energy-momentum conservation requires

$$(k_e-k_{e'})_\mu=q_\mu=(p'_N+P_{A-1}-P_A)_\mu , \tag{1}$$

i.e.,

$$\begin{aligned}&\mathbf{k}_e-\mathbf{k}_{e'}=\mathbf{Q}=\mathbf{p}'_N+\mathbf{P}_{A-1}-\mathbf{P}_A ,\\ &E_e-E_{e'}=\omega=E_{p'_N}+M_{A-1}^*-M_A^* .\end{aligned} \tag{2}$$

All evaluations are carried out in the target rest frame $P_A=(\mathbf{0};iM_A)$. Throughout this work we use the notations and conventions introduced by de Forest.[14]

The one-photon-exchange formalism, when applied to electron-nucleus scattering, nicely separates the known quantity, i.e., the electron-photon interaction from the unknown quantity, i.e., the photon-nucleus interaction, thereby taking full advantage of very general considerations of Lorentz covariance and gauge invariance. Since the interaction Hamiltonian is the contraction of the electron current and the vector potential arising from the nuclear current,

$$H(\mathbf{x},t)=-ej_\mu^{\text{electron}}(\mathbf{x})A_\mu^{\text{ext}}(\mathbf{x},t) , \tag{3}$$

the cross section turns out to be the contraction of two

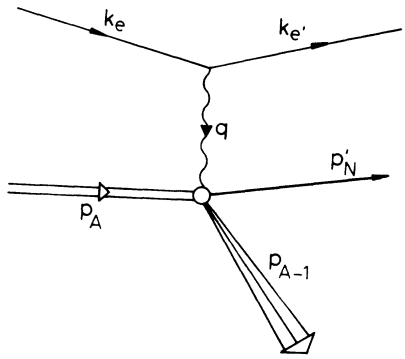

FIG. 1. Nuclear breakup into a single nucleon and a residual nuclear system due to electron scattering in Born approximation.

tensors. Hence, the most general cross section for the $A(e,e'p)A-1$ scattering process in the ultrarelativistic approximation for the electron, i.e., $k_{e_\mu}^2=0$, can be expressed as

$$\frac{d^4\sigma}{d\Omega_{k_{e'}}dE_{e'}d\Omega_{p'_N}dE_{p'_N}}=\frac{2\alpha^2}{q_\mu^4}\frac{k_{e'}}{k_e}p'_NE_{p'_N}\eta_{\mu\nu}W_{\mu\nu} , \tag{4}$$

where α is the fine structure constant and $q_\mu^2=\mathbf{Q}^2-\omega^2$ is the squared momentum-energy transfer. According to the above approximation $k_{e'}/k_e=E_{e'}/E_e$.

The electron-photon tensor $\eta_{\mu\nu}$ for unpolarized electron scattering is given by ($m_e^2\approx 0$)

$$\eta_{\mu\nu}=k_{e_\mu}k_{e'_\nu}+k_{e'_\mu}k_{e_\nu}+\tfrac{1}{2}q_\mu^2\delta_{\mu\nu} . \tag{5}$$

All the interesting information about the nucleus is contained in the nuclear structure tensor $W_{\mu\nu}$. Formally the nuclear structure tensor can be written as

$$\begin{aligned}W_{\mu\nu}=\overline{\sum_i}\sum_{f_R}\delta(E_{p'_N}+E_{f_R}-E_i-\omega)\langle f_R,\mathbf{p}'_N|J_{N_\mu}(q)|i\rangle\\ \times\langle f_R,\mathbf{p}'_N|J_{N_\nu}(q)|i\rangle^* ,\end{aligned} \tag{6}$$

where $i(f)$ and $E_i(E_f)$ refer to the initial (final) nuclear state and its energy. Asymptotically the final nuclear system is described by a product of a plane wave $|\mathbf{p}'_N\rangle$ for the detected nucleon and an eigenstate $|f_R\rangle$ for the residual nuclear system. Using relativistic kinematics the various energies in the lab frame are

$$\begin{aligned}&E_i=M_A ,\\ &E_{p'_N}=\sqrt{p'^2_N+M_N^2} ,\\ &E_{f_R}=\sqrt{(\mathbf{Q}-\mathbf{p}'_N)^2+M_{A-1}^{*2}}\\ &\quad\simeq\sqrt{(\mathbf{Q}-\mathbf{p}'_N)^2+M_{A-1}^2}+E_{A-1} .\end{aligned} \tag{7}$$

It is convenient to express the intrinsic energy of the pair by the separation or missing energy E_{miss}, which is an independent quantity,

$$E_{\text{miss}}=M_N+M_{A-1}^*-M_A . \tag{8}$$

Nonrelativistically, the missing energy becomes

$$E_{\text{miss}}=E_{A-1}-E_A \ . \tag{9}$$

It is convenient to choose a particular coordinate frame in order to express the breakup cross section in terms which can be identified directly with the various components of the nuclear current. Following de Forest[14] we choose a frame of reference which is determined by the momenta Q and $\mathbf{p}'_N$:

$$\begin{aligned}\hat{\mathbf{n}}_z&=\hat{\mathbf{Q}} \ ,\\ \hat{\boldsymbol{\eta}}_\perp&=\mathbf{Q}\times\mathbf{p}'_N/|\mathbf{Q}\times\mathbf{p}'_N| \ ,\\ \hat{\mathbf{n}}_\parallel&=\hat{\mathbf{n}}_\perp\times\mathbf{Q}/|\hat{\mathbf{n}}_\perp\times\mathbf{Q}| \ .\end{aligned} \tag{10}$$

In Fig. 2, γ is the angle between the transferred momentum Q and the outgoing nucleon $\mathbf{p}'_N$, and ϕ is the angle between the electron plane and the nucleonic plane

$$\cos\phi=\hat{\mathbf{n}}_\perp\cdot(\mathbf{k}_e\times\mathbf{k}_{e'})/|\mathbf{k}_e\times\mathbf{k}_{e'}| \ . \tag{11}$$

All calculations presented in this work are in-plane results, i.e., $\phi=0$ or $\phi=\pi$. The components of the nuclear current are defined with respect to this frame,

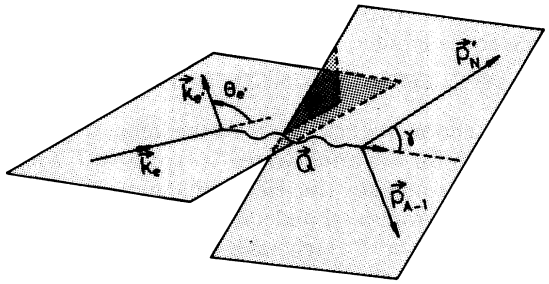

FIG. 2. Kinematic structure of $(e,e'p)$ reaction.

$$J_{N_\mu}=(\mathbf{J}_N;i\rho_N) \ , \tag{12}$$

where $J_{N_k}=\mathbf{J}_N\cdot\hat{\mathbf{n}}_k$, with $k=z,\perp,\parallel$. In this specific frame of reference the tensor product $\eta_{\mu\nu}W_{\mu\nu}$ from Eq. (4) can be written as a sum of four terms $v_j W_j$. The unpolarized breakup cross section becomes

$$\begin{aligned}\frac{d^4\sigma}{d\Omega_{k_{e'}}dE_{e'}d\Omega_{p'_N}dE_{p'_N}}=p'_N E_{p'_N}\sigma_{\text{Mott}}&\left[\frac{q_\mu^4}{\mathbf{Q}^4}W_C+\left[\frac{q_\mu^2}{2\mathbf{Q}^2}+\tan^2\tfrac{1}{2}\theta_{e'}\right]W_T+\frac{q_\mu^2}{\mathbf{Q}^2}\left[\frac{q_\mu^2}{\mathbf{Q}^2}+\tan^2\tfrac{1}{2}\theta_{e'}\right]^{1/2}W_I\cos\phi\right.\\&\left.+\left[\frac{q_\mu^2}{\mathbf{Q}^2}\cos^2\phi+\tan^2\tfrac{1}{2}\theta_{e'}\right]W_S\right] \ ,\end{aligned} \tag{13}$$

where

$$\sigma_{\text{Mott}}=4\alpha^2E_{e'}^2\cos^2(\tfrac{1}{2}\theta_{e'})/q_\mu^4$$

and $\theta_{e'}$ is the electron scattering angle $\cos\theta_{e'}=\hat{\mathbf{k}}_{e'}\cdot\hat{\mathbf{k}}_e$.

In this frame the nuclear structure functions can be expressed in shorthand notation as

$$\begin{aligned}W_C&=\langle\rho_N^2\rangle \ ,\\ W_T&=2\langle J_{N_\perp}^2\rangle \ ,\\ W_S&=\langle J_{N_\parallel}^2\rangle-\langle J_{N_\perp}^2\rangle \ ,\\ W_I&=-\langle\rho_N J_{N_\parallel}\rangle-\langle J_{N_\parallel}\rho_N\rangle \ ,\end{aligned} \tag{14}$$

where conservation of the nuclear current

$$\mathbf{Q}\cdot\mathbf{J}_N=\omega\rho_N \ , \tag{15}$$

is used to eliminate the nuclear current component J_{N_z} in favor of the nuclear charge density ρ_N. Elimination of the charge density yields instead of Eq. (14)

$$\begin{aligned}W_C&=\frac{Q^2}{\omega^2}\langle J_{N_z}^2\rangle \ ,\\ W_T&=2\langle J_{N_\perp}^2\rangle \ ,\\ W_S&=\langle J_{N_\parallel}^2\rangle-\langle J_{N_\perp}^2\rangle \ ,\\ W_I&=-\frac{Q}{\omega}\langle J_{N_z}J_{N_\parallel}\rangle-\frac{Q}{\omega}\langle J_{N_\parallel}J_{N_z}\rangle \ .\end{aligned} \tag{16}$$

The set of nuclear structure functions in Eqs. (14) and (16) are depending on four kinematic variables,

$$W=W(Q,\omega,p'_N,\gamma) \ . \tag{17}$$

The nuclear structure functions W_S and W_I vanish when the outgoing nucleon is moving parallel or opposite to the transferred photon.[15]

In this work we assume that the nuclear current is composed of one-body currents only. Ignoring the two-body components implies that we lose explicit gauge invariance, since the off-shell matrix elements of the one-body current operators are in general not conserved. As a consequence the two sets of structure functions in Eqs. (14) and (16) are no longer equivalent.

The general structure of the free nucleon current is

$$\bar{U}\Gamma_\mu U=i\bar{U}(\mathbf{p}')\left[\gamma_\mu(F_1+\kappa F_2)+i(p+p')_\mu\frac{\kappa F_2}{2M_N}\right]U(\mathbf{p}) \ , \tag{18}$$

where $U_s(\mathbf{p})$ is the four component Dirac spinor

$$U_s(\mathbf{p})=\left[\frac{E_p+M_N}{2E_p}\right]^{1/2}\begin{bmatrix}1\\ \boldsymbol{\sigma}\cdot\mathbf{p}/(E_p+M_N)\end{bmatrix}\chi_s \ . \tag{19}$$

Here, χ_s is a two-component Pauli spinor and the components of σ are the Pauli matrices. F_1 and F_2 are the electromagnetic form factors of the nucleon, depending

only on q^2. In all calculations we have used the parametrization of Höhler *et al.*[16] for the $F_n's$. Various other parametrizations were found to lead to the same results. Assuming energy-momentum conservation at the photon-nucleon vertex, it is convenient to eliminate the vector $(p+p')_\mu$ in favor of $\sigma_{\mu\nu}(p-p')_\nu=-\sigma_{\mu\nu}q_\nu$ by means of the Gordon reduction of the current and we write down the equivalent current

$$\bar{U}\Gamma_\mu U=i\bar{U}(\mathbf{p}')\left[\gamma_\mu F_1-\sigma_{\mu\nu}q_\nu\frac{\kappa F_2}{2M_N}\right]U(\mathbf{p})\ . \tag{20}$$

In case the initial or final nucleon are off-mass-shell the most general nucleon current will contain considerably more structure[17] and one needs more than two types of operators in order to construct the nucleon current. Also the electromagnetic form factors will be modified in going off the mass shell.[18] Although the construction of a consistent and unambiguous one-body current should certainly be addressed as a serious conceptual problem, we shall not discuss it here. A detailed analysis of this problem can be found in Ref. 19. In this work, we use a one-body current which, on the one hand, does not violate the basic requirements like current conservation, four-momentum conservation, and Lorentz invariance too severe and, on the other hand, can be put into practice rather easily. In the description of de Forest[14] the nucleons are still represented by free Dirac spinors, although one nucleon is initially bound. As a consequence energy conservation at the vertex is no longer satisfied, i.e.,

$$\bar{\omega}\neq\omega\ , \tag{21}$$

with

$$\begin{aligned}&\bar{\omega}=E'-E,\quad E'=\sqrt{p'^2+M_N^2}\ ,\\ &E=\sqrt{p^2+M_N^2},\quad \mathbf{p}'=\mathbf{p}+\mathbf{Q}\ .\end{aligned} \tag{22}$$

Consequently the currents in Eqs. (18) and (20) are no longer equivalent. We restate the first current analogous to the second current,

$$\bar{j}_\mu=i\bar{U}(\mathbf{p}')\left[\gamma_\mu F_1-\sigma_{\mu\nu}\bar{q}_\nu\frac{\kappa F_2}{2M_N}\right]U(\mathbf{p})\ , \tag{23}$$

$$j_\mu=i\bar{U}(\mathbf{p}')\left[\gamma_\mu F_1-\sigma_{\mu\nu}q_\nu\frac{\kappa F_2}{2M_N}\right]U(\mathbf{p})\ , \tag{24}$$

where $\bar{q}_\nu=(\mathbf{Q};i\bar{\omega})$. As the initially bound nucleon is described by free Dirac spinors, the current is also no longer conserved due to $q_\mu\bar{U}(\mathbf{p}')\gamma_\mu U(\mathbf{p})\neq 0$. The lack of gauge invariance is restored in an *ad hoc* way, i.e., by eliminating the longitudinal component j_Q in favor of the charge. The advantage of the current in Eq. (24) is that the $\sigma_{\mu\nu}q_\nu$ term is already gauge invariant, whereas the $\sigma_{\mu\nu}\bar{q}_\nu$ term is not. The argument to eliminate j_Q rather than ρ is given by the generally accepted assumption that the predictions for the charge density are better understood. More detailed arguments are given by de Forest.[14]

The actual nuclear breakup calculations are done in the momentum representation. Computing the current matrix elements requires expressions which explicitly show the momentum dependence. Before doing so we first discuss the difference between the currents expressed in Eqs. (23) and (24). Since

$$\bar{q}_\mu-q_\mu=[0;i(\bar{\omega}-\omega)]\ ,$$

they differ only in the current components

$$\bar{j}_\mu-j_\mu=\bar{U}(\mathbf{p}')\left[\sigma_{\mu 4}(\bar{\omega}-\omega)\frac{\kappa F_2}{2M_N}\right]U(\mathbf{p})\ . \tag{25}$$

Due to the antisymmetry of $\sigma_{\mu\nu}$, $\bar{\rho}=\rho$. The gauge invariance prescription subsequently implies that $\bar{W}_C=W_C$. The derivation of the current amplitudes is straightforward. It requires the evaluation of the matrix elements $\bar{U}U$, $\bar{U}\gamma_k U$, $\bar{U}\gamma_4 U$, and $\bar{U}\gamma_4\gamma_k U$. With these, we can derive the current matrix elements, which manifestly depend on the nucleon momenta $\mathbf{p}'$ and $\mathbf{p}$ and the four-momentum transfer q_μ. In doing so, we use the following notation:

$$\langle \mathbf{p}'s'|j_k|\mathbf{p}s\rangle=\chi^\dagger_{s'}(S^0_k+i\mathbf{S}_k\boldsymbol{\sigma})\chi_s\ , \tag{26}$$

$$\langle \mathbf{p}'s'|\rho|\mathbf{p}s\rangle=\chi^\dagger_{s'}(S^0_\rho+i\mathbf{S}_\rho\boldsymbol{\sigma})\chi_s\ , \tag{27}$$

where j_k stands for $\mathbf{j}\cdot\hat{\mathbf{n}}_k$ $(k=z,\|,\perp)$. The explicit expressions for the components S of the barred current in Eq. (23) are

$$\begin{aligned}
\bar{S}^{\,0}_\rho&=c(E',E)\left\{[(E'+M_N)(E+M_N)+\mathbf{p}\cdot\mathbf{p}'](F_1+\kappa F_2)-(E'+E)[(E'+M_N)(E+M_N)-\mathbf{p}\cdot\mathbf{p}']\frac{\kappa F_2}{2M_N}\right\},\\
\bar{S}^{\,l}_\rho&=c(E',E)\left\{[(\mathbf{p}'\times\mathbf{p})\cdot\hat{\mathbf{n}}_l]\left[F_1+\kappa F_2+(E'+E)\frac{\kappa F_2}{2M_N}\right]\right\},\\
\bar{S}^{\,0}_k&=c(E',E)\left\{[(E'+M_N)\mathbf{p}\cdot\hat{\mathbf{n}}_k+(E+M_N)\mathbf{p}'\cdot\hat{\mathbf{n}}_k](F_1+\kappa F_2)-[(\mathbf{p}'+\mathbf{p})\cdot\hat{\mathbf{n}}_k][(E'+M_N)(E+M_N)-\mathbf{p}\cdot\mathbf{p}']\frac{\kappa F_2}{2M_N}\right\},\\
\bar{S}^{\,l}_k&=c(E',E)\left[\{[(E'+M_N)\hat{\mathbf{n}}_k\times\mathbf{p}+(E+M_N)\mathbf{p}'\times\hat{\mathbf{n}}_k]\cdot\hat{\mathbf{n}}_l\}(F_1+\kappa F_2)+[(\mathbf{p}'+\mathbf{p})\cdot\hat{\mathbf{n}}_k][(\mathbf{p}'\times\mathbf{p})\cdot\hat{\mathbf{n}}_l]\frac{\kappa F_2}{2M_N}\right].
\end{aligned} \tag{28}$$

The lower index labels the component of the current, while the upper index labels the component of the Pauli spin matrix ($l=z,\|,\perp$). The common factor $c(E',E)$ is given by

$$c(E',E)=\frac{1}{\sqrt{4E'E(E'+M_N)(E+M_N)}} . \tag{29}$$

From the barred components $\bar{S}$, we can easily derive the unbarred components S, which refer to the current in Eq. (24):

$$\begin{aligned}
S^0_\rho &= \bar{S}^{\,0}_\rho , \\
S^l_\rho &= \bar{S}^{\,l}_\rho , \\
S^0_k &= \bar{S}^{\,0}_k + c(E',E)[(E'+M_N)\mathbf{p}\cdot\hat{\mathbf{n}}_k-(E+M_N)\mathbf{p}'\cdot\hat{\mathbf{n}}_k] \\
&\quad\times(\omega-\bar{\omega})\frac{\kappa F_2}{2M_N} , \\
S^l_k &= \bar{S}^{\,l}_k - c(E',E)(\{[(E+M_N)\mathbf{p}'+(E'+M_N)\mathbf{p}] \\
&\quad\times\hat{\mathbf{n}}_k\}\cdot\hat{\mathbf{n}}_l)(\omega-\bar{\omega})\frac{\kappa F_2}{2M_N} .
\end{aligned} \tag{30}$$

In order to get a better understanding of the several current components we make a nonrelativistic reduction by expanding the quantities S in a series in parameter $1/M_N$. Up to order $1/M_N^2$ we find

$$\begin{aligned}
S^0_\rho &= F_1-(F_1+2\kappa F_2)Q^2/8M_N^2+\mathcal{O}\left(\frac{1}{M_N^4}\right) , \\
S^l_\rho &= (F_1+2\kappa F_2)[\mathbf{Q}\times\mathbf{p}'\cdot\hat{\mathbf{n}}_l]/4M_N^2+\mathcal{O}\left(\frac{1}{M_N^4}\right) , \\
S^0_k &= F_1(2\mathbf{p}'-\mathbf{Q})\cdot\hat{\mathbf{n}}_k/2M_N+\mathcal{O}\left(\frac{1}{M_N^3}\right) , \\
S^l_k &= (F_1+\kappa F_2)[(\mathbf{Q}\times\hat{\mathbf{n}}_k)\cdot\hat{\mathbf{n}}_l)/2M_N+\mathcal{O}\left(\frac{1}{M_N^3}\right) .
\end{aligned} \tag{31}$$

These nonrelativistic expressions are valid for both currents since we assume that $\bar{\omega}-\omega$ is of order $1/M_N$, and consequently the current difference is of order $(1/M_N^3)$. The dominant term clearly is the direct charge contribution F_1 occurring in S^0_ρ. The leading terms in S_k are recognized as the convection current (S^0_k) and the rotation of the intrinsic spin magnetization $\nabla\times\hat{\boldsymbol{\mu}}(\mathbf{x})$ (the term S^l_k). The $1/M_N^2$ contributions in S_ρ are the well known Darwin-Foldy term (remaining part S^0_ρ) and spin-orbit terms (S^l_ρ).

B. Off-shell electron-nucleon cross sections

The plane wave impulse approximation (PWIA) model offers the possibility to make a further analysis of the electromagnetic part. This approximation assumes that the outgoing nucleon is directly knocked into a final plane wave state $|\mathbf{p}'_N\sigma'_N\tau'_N\rangle$. Consequently the electromagnetic interaction factorizes from the complicated nuclear overlap and we can express the PWIA cross section as

$$\frac{d^4\sigma}{d\Omega_{e'}dE_{e'}d\Omega_{p'_N}dE_{p'_N}}=p'_NE_{p'_N}\sigma_{eN}S(|\mathbf{p}'_N-\mathbf{Q}|,E_m) . \tag{32}$$

The nuclear spectral function $S(\mathbf{p}_m,E_m)$ will be discussed in Sec. IV. The quantity σ_{eN} is the (half) off-shell electron-nucleon cross section, first introduced in Ref. 20,

$$\sigma_{eN}=\sigma_{\text{Mott}}(v_Cw_C+v_Tw_T+v_Sw_S+v_Iw_I) , \tag{33}$$

where the electron-photon factors v are expressed in Eq. (13). Like the $\eta_{\mu\nu}$ components the tensor $w_{\mu\nu}$ follows readily from

$$w_{\mu\nu}=\frac{1}{2}\sum_{s's}\langle\mathbf{p}'s'|\Gamma_\mu|\mathbf{p}s\rangle\langle\mathbf{p}'s'|\Gamma_\nu|\mathbf{p}s\rangle^* . \tag{34}$$

de Forest[14] presents a detailed discussion of certain classes of (half) off-shell eN cross sections. Therefore we suffice with stating the final results for the relevant combinations of the photon-nucleon tensor:

$$\begin{aligned}
\bar{w}_C &= \frac{1}{4EE'}\left[(E+E')^2\left[F_1^2+\frac{\bar{q}_\mu^{\,2}}{4M_N^2}\kappa^2F_2^2\right]\right. \\
&\quad\left.-\mathbf{Q}^2(F_1+\kappa F_2)^2\right] , \\
\bar{w}_T &= \frac{1}{2EE'}\bar{q}_\mu^{\,2}(F_1+\kappa F_2)^2 , \\
\bar{w}_S &= \frac{1}{EE'}p'^2_N\sin^2\gamma\left[F_1^2+\frac{\bar{q}_\mu^{\,2}}{4M_N^2}\kappa^2F_2^2\right] , \\
\bar{w}_I &= -\frac{1}{EE'}p'_N\sin\gamma(E+E')\left[F_1^2+\frac{\bar{q}_\mu^{\,2}}{4M_N^2}\kappa^2F_2^2\right] .
\end{aligned} \tag{35}$$

Equations (35) are the functions which correspond to the current from Eq. (23). The energies E and E' are the energies of the nucleon before and after the electromagnetic interaction. Equation (24) leads to

$$\begin{aligned}
w_C &= \bar{w}_C , \\
w_T &= \frac{1}{EE'}\left\{-(p_\mu p'_\mu+M_N^2)F_1^2+\bar{q}_\mu q_\mu F_1\kappa F_2\right. , \\
&\quad\left.+[2p_\mu q_\mu p'_\nu q_\nu-(p_\mu p'_\mu-M_N^2)q_\mu^2]\frac{\kappa^2F_2^2}{4M_N^2}\right\} , \\
w_S &= \frac{1}{EE'}p'^2_N\sin^2\gamma\left[F_1^2+\frac{q_\mu^2}{4M_N^2}\kappa^2F_2^2\right] , \\
w_I &= \frac{1}{EE'}p'_N\sin\gamma\left\{-(E+E')F_1^2\right. \\
&\quad+[(p+p')_\mu q_\mu\omega-(E+E')q_\mu^2] \\
&\quad\left.\times\frac{\kappa^2F_2^2}{4M_N^2}\right\} .
\end{aligned} \tag{36}$$

The nonrelativistic reduction of the current leads to

$$
\begin{aligned}
w_C^{\rm nr} &= F_1^2 - F_1(F_1+2\kappa F_2)\mathbf{Q}^2/4M_N^2 + \mathcal{O}\left[\frac{1}{M_N^4}\right], \\
w_T^{\rm nr} &= (F_1+\kappa F_2)^2\mathbf{Q}^2/2M_N^2 + \mathcal{O}\left[\frac{1}{M_N^4}\right], \\
w_S^{\rm nr} &= p_N'^2\sin^2\gamma F_1^2/M_N^2 + \mathcal{O}\left[\frac{1}{M_N^4}\right], \\
w_I^{\rm nr} &= -2p_N'\sin\gamma F_1^2/M_N + \mathcal{O}\left[\frac{1}{M_N^3}\right].
\end{aligned}
\tag{37}
$$

Like de Forest[14] we may consider the implications of using different currents for the resulting off-shell cross sections. The results are plotted in Fig. 3. For reasons of comparison we have added a completely different off-shell cross section σ^S, which has been extensively used by the Saclay group for a couple of years. σ^S is originally introduced by Mougey[21] and results from a different conceptual approach. At present most groups, including the Saclay group, employ one of the cross sections $\sigma^{\rm cc}$ expressed in Eq. (35) or Eq. (36). In calculating the various σ_{eN} cross sections we have confined the kinematics to regions which are of interest for the two-body breakup reaction of ^{3}He. The separation energy $E_s = 5.5$ MeV, while the recoil

$$E_{\rm rec} = [(\mathbf{Q}-\mathbf{p}_N')^2 + 4M_N^2]^{1/2} .$$

The four sets of (Q, E_{el}) points are more or less representative for the current experimental situation. Furthermore, increasing the electron energy does decrease the differences. Figure 3 clearly shows that there is no significant difference between $\sigma_1^{\rm cc}$ of Eq. (35) and $\sigma_2^{\rm cc}$ of Eq. (36) in any of the kinematic regions. On the other hand, σ^S and $\sigma^{\rm nr}$ show a rather large discrepancy with the $\sigma^{\rm cc}$ set. For the large Q value, $\sigma^{\rm nr}$ is not even close to $\sigma^{\rm cc}$ at the most on-shell point, $\gamma = 0$. The issue of current conservation poses a more serious problem. Instead of using the set of W functions from Eq. (14) we calculated the half-off-shell cross section from Eq. (16), in which the current component J_{N_Q} is kept rather than the charge ρ_N. The results are quite different. It should, however, be noted that the prescription of eliminating the charge operator has the drawback that it cannot be applied for the elastic charge form factors, in view of the factor ω in Eq. (15). In view of the close similarity of $\sigma_1^{\rm cc}$ and $\sigma_2^{\rm cc}$ we decided to make a definite choice for one of them. Since the current amplitudes in Eq. (28), which lead to $\sigma_1^{\rm cc}$, have the simplest structure, we performed the calculations with the current of Eq. (23). But this choice merely is a matter of taste. In order to resolve the problem of gauge invariance violation it is clear that the question of off-shell dependence deserves to be investigated in detail.

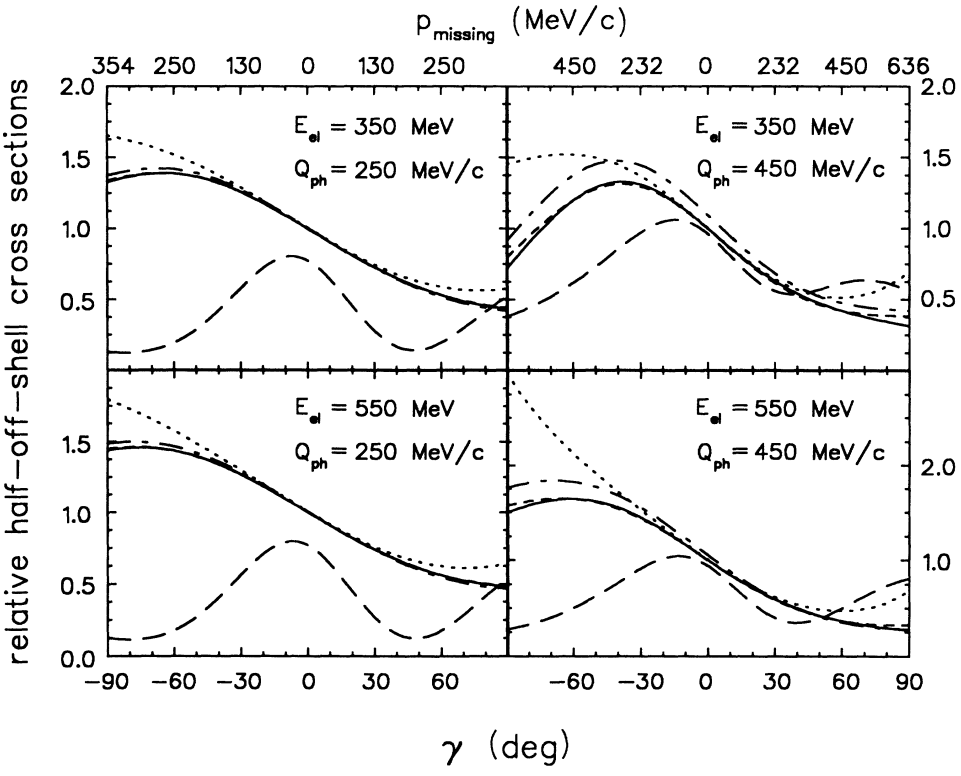

FIG. 3. Half-off-shell electron-nucleon cross sections. The solid and short-dashed curves represent the cross sections $\sigma_1^{\rm cc}$ and $\sigma_2^{\rm cc}$ from, respectively, Eqs. (35) and (36). The dashed-dotted curve shows the cross section $\sigma^{\rm nr}$ [Eq. (37)], while the dotted curve shows the cross section σ^S (Ref. 21). In the long-dashed curve the current component J_{N_Q} is kept instead of the charge ρ_N.

TABLE I. Parameters of MT I-III potential (Ref. 12).

MT I-III	$^1S_0$	$^3S_1$
μ_A ($\sqrt{\text{MeV}}$)	10	10
λ_A ($\sqrt{\text{MeV}}$)	4.1	4.996
μ_R ($\sqrt{\text{MeV}}$)	20	20
λ_R ($\sqrt{\text{MeV}}$)	11.48	11.48

In such studies physically reasonable dynamical models with proper gauge invariance properties have to be considered.

III. THREE-NUCLEON DYNAMICS

In this section we present explicit forms for the half-off-shell $NNN \rightarrow Nd$ scattering wave function and the trinucleon bound state wave function, which are needed in the electromagnetic analysis of the two-body breakup reaction of the $A=3$ system. The wave functions are constructed from the Faddeev amplitudes, which are determined by solving the Faddeev equations. The relative momenta and spin-isospin quantum numbers, which label the various three-nucleon states are defined and discussed in Appendix A. For purposes of numerical evaluation we have adopted the separable UPE method (Appendix B) to describe a realistic local s-wave spin-dependent potential. It is known that already the first term of this expansion, i.e., the unitary pole approximation (UPA), gives a fair description of the trinucleon binding energy.[22,23] To determine the validity of the UPE method in the scattering region we have studied the UPE convergence properties of the Nd scattering observables. In the remainder of this paper all formulas are written down for the simple case of the UPA. Extension to UPE is straightforward.

The local potential we have adopted as NN input is the Malfliet-Tjon (MT) potential, set I-III.[12] In both channels it is described by a spin-dependent central Yukawa-type interaction

$$V(r)=-\frac{\lambda_A e^{-\mu_A r}}{r}+\frac{\lambda_R e^{-\mu_R r}}{r} . \tag{38}$$

Despite its simplicity it gives a surprisingly good fit to the two-nucleon scattering observables. To be self-contained we list its parameters in Table I. The UPE eigenvalues for this potential, obtained according to Eq. (B2), are listed in Table II.

Hereafter we characterize the type of approximation made in the UPE as $(ntp,ntm)^3S_1,(ntp,ntm)^1S_0$, where $ntp(ntm)$ refers to the number of positive (negative) eigenvalues retained in the expansion. For example, UPA is (1010). To study the convergence rate of the separable expansion in the scattering region we computed the NN phase shift parameters in both channels and compared their values with the phase shift parameter obtained with the local potential. The results are shown in Fig. 4. The number of retained eigenvalues is increased from (10)-UPA to (53)-UPE. The deviation between the result calculated with the (53)-UPE expansion and the local result is merely numerical inaccuracy. Also the (22)-UPE expansion gives a satisfactory description, which is an important result, since the three-body codes are updated for at most eight eigenvalues. The UPA results are not that good, but still reasonable, at least in the low-energy region. Note that in the singlet channel the UPA result for $s=E_d$ shows a better convergence than the $s=0$ curve. This result is somewhat surprising in view of the fact that the latter choice clearly exhibits a larger first eigenvalue. Apparently this in itself does not guarantee a better convergence to the local T matrix.

The multiple scattering series for the three-body system is constructed from the subsequent iteration of the Faddeev equations (Appendix C). In diagrammatic form, this series can be represented as in Fig. 5. The corresponding scattering wave function can be written as

$$f(\mathbf{p},\mathbf{q};\beta|d,\mathbf{q}_f;\beta_f)=\sum_{n=0}^{\infty} B^{(n)}(\mathbf{p},\mathbf{q};\beta|d,\mathbf{q}_f;\beta_f) , \tag{39}$$

where $\mathbf{p},\mathbf{q}$ denote off-shell momenta. The first diagram in Fig. 5 is called the disconnected term. The corresponding lowest order term $B^{(0)}$ is not included in Eq. (C12) and will be treated separately from the rest, since it contains a delta function for the spectator part. Its form is

$$B^{(0)}(\mathbf{p}_1,\mathbf{q}_1;\beta_1|d,\mathbf{q}_f;\beta_f)=\delta(\mathbf{q}_1-\mathbf{q}_f)\phi_d(\mathbf{p}_1)\delta_{\beta_1\beta_f} , \tag{40}$$

where ϕ_d is the normalized deuteron wave function expressed in Eq. (B4).

The next term $B^{(1)}$ is connected and will serve as the driving term of the multiple scattering series. Indeed, this term is proportional to the inhomogeneous term in Eq. (C12).

We drop the antisymmetrization label in Eq. (C12), keeping in mind that the scattering only affects subsys-

TABLE II. UPE eigenvalues.

	$^3S_1$, $s=E_d$		$^1S_0$, $s=E_d$		$^1S_0$, $s=0$	
λ-UPE	$\lambda>0$	$\lambda<0$	$\lambda>0$	$\lambda<0$	$\lambda>0$	$\lambda<0$
1	1	−1.970 470	0.626 569	−2.605 216	0.926 828	−2.685 485
2	0.159 329	−0.367 408	0.097 967	−0.534 540	0.114 680	−0.537 293
3	0.061 723	−0.075 586	0.037 879	−0.143 338	0.041 807	−0.143 557
4	0.032 556		0.019 956	−0.027 930	0.021 438	−0.027 955
5	0.025 143		0.012 373		0.013 080	

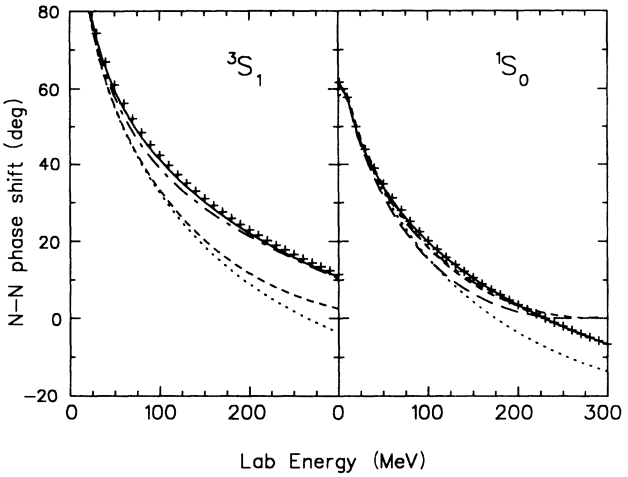

FIG. 4. *NN* phase shift parameter δ_0. The crosses represent the result for the local MT interaction, set I-III (Ref. 12). The curves show the results for the various UPE combinations. The short-dashed curve corresponds to UPA, the dotted curve to (11)-UPE, the long-dashed–dotted curve to (22)-UPE, and the solid curve to (53)-UPE. The long-dashed curve present only in the figure for the singlet parameter results from a UPA calculation with the s value set to 0.

tems with definite parity $(-)^{l_p+s_p+t_p}=-1$. Inserting the UPA form of Eq. (B8) for the two-particle T matrix, we can express $B^{(1)}$ as

$$B^{(1)}(\mathbf{p}_1,\mathbf{q}_1;\beta_1|d,\mathbf{q}_f;\beta_f)\sim g(p_1;\beta_1)\tau(z-q_1^2;\beta_1)\times\Psi^{(1)}(\mathbf{q}_1;\beta_1|\mathbf{q}_f;\beta_f)\ , \tag{41}$$

where

$$\Psi^{(1)}(\mathbf{q}_1;\beta_1|\mathbf{q}_f;\beta_f)=\int d\mathbf{p}_n' d\mathbf{q}_n' g(p_1';\beta_1)\times\delta(\mathbf{q}_1-\mathbf{q}_1')\,{}_1\langle\beta_1|\beta_f\rangle_3\times\phi_d(p_3')\delta(\mathbf{q}_3'-\mathbf{q}_f)\ . \tag{42}$$

The β dependence of the functions g and τ is understood to refer only to the spin s_p of the relevant subsystem.

The momenta $\mathbf{p}_1'$ and $\mathbf{p}_3'$ are expressed into $\mathbf{q}_1'$ and $\mathbf{q}_3'$ and the index n in Eq. (42) is fixed to 1 or 3. The result of the integrations becomes

$$\Psi^{(1)}(\mathbf{q}_1;\beta_1|\mathbf{q}_f;\beta_f)=2(2/\sqrt{3})^3\,{}_1\langle\beta_1|\beta_f\rangle_3\times g\left[\frac{2}{\sqrt{3}}|\mathbf{q}_f+\tfrac{1}{2}\mathbf{q}_1|;\beta_1\right]\times\phi_d\left[\frac{2}{\sqrt{3}}|\mathbf{q}_1+\tfrac{1}{2}\mathbf{q}_f|\right]\ . \tag{43}$$

This term is called the rescattering contribution. For each disconnected diagram there are two rescattering diagrams and $\Psi^{(1)}$ is multiplied by a factor 2. We may now perform a partial wave decomposition

$$\Psi_l^{(1)}(q_1;\beta_1|q_f;\beta_f)=\frac{1}{2}\int_{-1}^{+1}dx_{1f}P_l(x_{1f})\Psi^{(1)}(\mathbf{q}_1;\beta_1|\mathbf{q}_f;\beta_f)\ . \tag{44}$$

The $(n+1)$th term of the multiple scattering series can be found from the nth order wave function using the resulting partial wave decomposed equation

$$\Psi_l^{(n+1)}(q_1;\beta_1|q_f;\beta_f)=-8\pi\sum_{\beta'}\int dq_3' q_3'^2 K_l(q_1;\beta_1|q_3';\beta')\tau(z-q_3'^2;\beta')\Psi_l^{(n)}(q_3';\beta'|q_f;\beta_f)\ , \tag{45}$$

where the kernel is given by

$$K_l(q_1;\beta|q_3';\beta')=\frac{4}{3\sqrt{3}}\int dx_{13}'P_l(x_{13}')\frac{g(2/\sqrt{3}|\mathbf{q}_3'+\frac{1}{2}\mathbf{q}_1|;\beta)\,{}_1\langle\beta|\beta'\rangle_3 g(2/\sqrt{3}|\mathbf{q}_1+\frac{1}{2}\mathbf{q}_3'|;\beta')}{\frac{4}{3}(q_1^2+q_3'^2+q_1q_3'x_{13}')-z}\ . \tag{46}$$

The recoupling coefficients in Eqs. (43) and (46) can be found using Eqs. (A19) and (A21). In spin doublet scattering we have ${}_1\langle\chi_t^d\eta_s^d|\chi_s^d\eta_t^d\rangle_3={}_1\langle\chi_s^d\eta_t^d|\chi_t^d\eta_s^d\rangle_3=-\frac{3}{4}$ and ${}_1\langle\chi_t^d\eta_s^d|\chi_t^d\eta_s^d\rangle_3={}_1\langle\chi_s^d\eta_t^d|\chi_s^d\eta_t^d\rangle_3=\frac{1}{4}$. In spin quartet scattering we have ${}_1\langle\chi_t^q\eta_s^d|\chi_t^q\eta_s^d\rangle_3=-\frac{1}{2}$. In the (numerical) analysis of the Eqs. (46) and (45) one encounters serious problems due to the presence of various singularities in the integrand. A correct treatment of these singularities is essential. The resolvent in Eq. (46) contains a pole of type $(x-x_s)^{-1}$ due to the scattering of three free particles. The evaluation of Eq. (46) gives rise to logarithmic discontinuities in the integrand of Eq. (45), which emerge at the threshold of the three-particle scattering region. Furthermore, this equation has a deuteron-pole singularity of the form $[q_3'^2-(s_{\text{c.m.}}-E_d)]^{-1}$. In the numerical evaluations the method of subtraction techniques is used in order to remove the three types of singularities. This method is described in detail in Ref. 13.

After the partial wave components of $\Psi^{(n+1)}$ have been calculated, the final-state wave function stated in Eq. (39) can be reconstructed as

$$f(\mathbf{p}_1,\mathbf{q}_1;\beta_1|d,\mathbf{q}_f;\beta_f)=\delta(\mathbf{q}_1-\mathbf{q}_f)\delta_{\beta_1\beta_f}\phi_d(\mathbf{p}_1)-\frac{1}{p_1^2+q_1^2-z}g(p_1;\beta_1)\tau(z-q_1^2;\beta_1)\sum_{l=0}^{\infty}(2l+1)P_l(\hat{\mathbf{q}}_1\cdot\hat{\mathbf{q}}_f)\sum_{n=1}^{\infty}\Psi_l^{(n)}(q_1;\beta_1|q_f;\beta_f)\ , \tag{47}$$

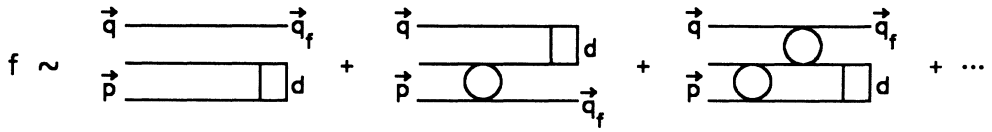

FIG. 5. Scattering series in diagrammatic form.

where the energy argument z corresponds to $s_{\text{c.m.}}+i\varepsilon$.

The solution to the half-off-shell *NNN-Nd* scattering wave function is reconstructed from the multiple scattering series at a given momentum point by using diagonal Padé approximants.[24] In general similar orders of approximants as for the on shell case studied in Ref. 13 are needed to find the converged solution. The found wave function was explicitly checked to be the solution of the integral equation by substituting it back in the equation. The numerical agreement at the mesh points of the q_1 grid was found to be excellent. Of course, due to the discretization, the numerical solution is only an approximation of the actual solution, but except for very small spectator momenta, the numerical solution is hardly sensitive for variations of the mesh parameters. Going to higher energies or to higher partial waves leads to more rapid convergence.

The relevant *Nd* scattering observables are the inelasticity η and phase shift parameter δ. In order to study the convergence properties of the UPE method, we have calculated these observables for various UPE combinations. To cover the kinematics scanned in the electromagnetic breakup, we have extended the energy range up to 150 MeV neutron lab energy, which corresponds with a T_{Nd} of roughly 100 MeV. To determine the rate of convergence the same observables were calculated for the local MT potential. In doing so we used the numerical analysis developed by Kloet.[13]

The results for the UPE phase parameters for the partial wave numbers $l=0$, 1, and 2 are summarized in the Figs. 6 and 7. In case of doublet scattering the calculations are carried out for the (1010)-UPE, (1111)-UPE, and (2222)-UPE combinations. Similarly for quartet scattering (10)-UPE, (11)-UPE, and (22)-UPE. The figures also show results for the phase shift and inelasticity parameters obtained with the local potential. In addition the local results are summarized in Table III. Small differences with previous low energy results[13] are due to improved numerical accuracy. The results beyond $E_{\text{lab}}=50$ MeV are new. Due to the expansion of the potential in terms

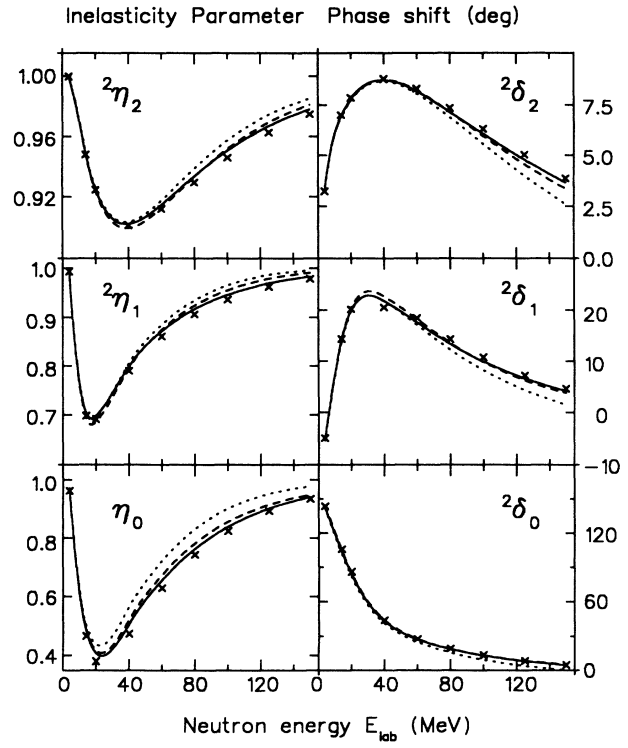

FIG. 6. *Nd* phase shift δ (degrees) and inelasticity η. Plotted are the results for doublet scattering in the partial wave numbers $l=0$, 1, and 2. The crosses account for the local results. The UPA, (1111)-UPE, and (2222)-UPE results are, respectively, represented by the dashed, dotted, and solid curves.

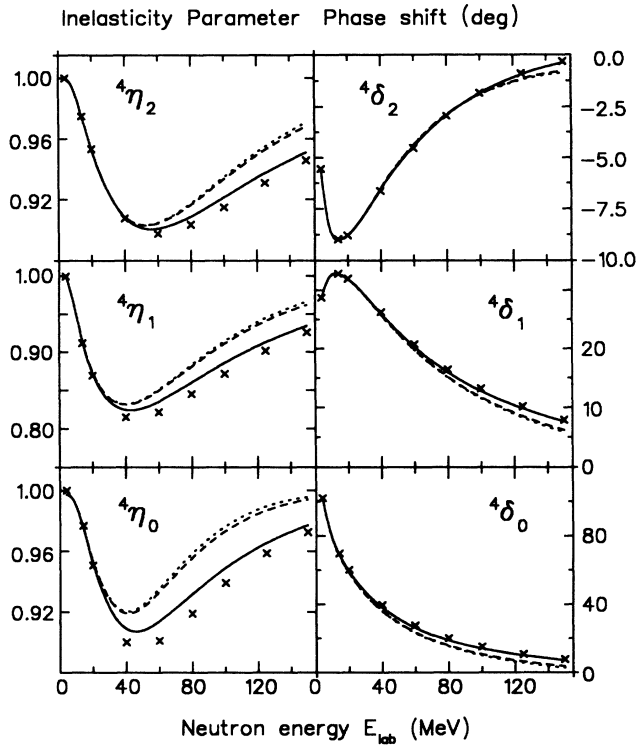

FIG. 7. *Nd* phase shift δ (degrees) and inelasticity η. Plotted are the results for quartet scattering in the partial wave numbers $l=0$, 1, and 2. The crosses account for the local results. The UPA, (11)-UPE, and (22)-UPE results are, respectively, represented by the dashed, dotted, and solid curves.

TABLE III. *Nd* phase shift δ (degrees) and inelasticity η for the partial waves $l=0$, 1, and 2, obtained with the local MT interaction, set I-III.

			Doublet parameters			
E_{lab}	$^2\delta_0$	$^2\eta_0$	$^2\delta_1$	$^2\eta_1$	$^2\delta_2$	$^2\eta_2$
4	143.62	0.962	−4.90	0.994	3.23	1.000
14.1	106.18	0.467	14.34	0.698	7.01	0.948
20	86.04	0.380	20.17	0.691	7.85	0.925
40	43.98	0.475	20.53	0.790	8.75	0.901
60	27.63	0.629	18.46	0.861	8.29	0.912
80	18.79	0.743	14.26	0.906	7.35	0.929
100	13.05	0.824	10.74	0.937	6.30	0.946
125	8.14	0.892	7.26	0.963	5.02	0.963
150	4.67	0.934	4.60	0.979	3.86	0.975
			Quartet parameters			
E_{lab}	$^4\delta_0$	$^4\eta_0$	$^4\delta_1$	$^4\eta_1$	$^4\delta_2$	$^4\eta_2$
4	102.13	1.000	28.73	1.000	−5.55	1.000
14.1	69.83	0.977	32.79	0.912	−8.97	0.975
20	60.21	0.951	31.92	0.869	−8.79	0.953
40	39.69	0.900	26.24	0.815	−6.63	0.908
60	27.73	0.901	20.74	0.821	−4.53	0.898
80	20.08	0.919	16.46	0.845	−2.95	0.903
100	14.95	0.939	13.21	0.871	−1.84	0.915
125	10.62	0.959	10.18	0.901	−0.91	0.931
150	7.67	0.973	7.93	0.926	−0.32	0.946

of (virtual) bound state components, one might expect that the UPE method loses accuracy at higher energies. Indeed, we observe a growing discrepancy between the local result and the lowest-order UPE results. Increasing the number of UPE terms leads to a much better convergence, but still the (22) term for $S=\frac{3}{2}$ or the (2222) term for $S=\frac{1}{2}$ are not able to give an exact reproduction of the local parameters. For the quartet $l=0$ scattering we have studied the UPE convergence up to eight eigenfunctions. The result is shown in Fig. 8. Indeed the (53) result has converged to the local parameters.

In the calculations of the electromagnetic breakup cross sections of the $A=3$ system, we evidently also need the wave function of the trinucleon bound state. Using an *s*-wave *NN* potential in UPA, the determination of the Faddeev amplitudes for the bound state becomes almost trivial. In contrast to the scattering states, which contain many partial wave components, the trinucleon bound state has definite total angular momentum $J=\frac{1}{2}$. Coupling the spin S to values $\frac{1}{2}$ or $\frac{3}{2}$ restricts the possible values of the orbital angular momentum L to 0 or 2. The value $L=1$ is excluded, since it violates parity. Furthermore $l_q=L$, since $l_p=0$. In the following evaluation we drop the $l_q=2$ component. Its contribution is very small and can easily be added, since it acts in just one channel with definite symmetry. Consequently the total three-nucleon spin S is restricted to the doublet value.

Application of the same scheme presented in the previous sections yields a one-dimensional homogeneous integral equation coupled in two channels,

$$\phi(q;\beta|E_B)=-\lambda_B\sum_{\beta'=1}^{2}\int dq'q'^2W(q;\beta|q';\beta')\times\tau(E_B-q^2;\beta')\times\phi(q';\beta'|E_B)\,, \tag{48}$$

where the kernel is given by

$$W(q,\beta|q';\beta')=8\pi(2/\sqrt{3})^3\tfrac{1}{2}\int_{-1}^{+1}dx\frac{g(2/\sqrt{3}|\frac{1}{2}\mathbf{q}+\mathbf{q}'|;\beta)\,{}_3\langle\beta|\beta'\rangle_1\,g(2/\sqrt{3}|\frac{1}{2}\mathbf{q}'+\mathbf{q}|;\beta')}{\frac{4}{3}(q'^2+q^2+qq'x)-E_B}\,. \tag{49}$$

The full Faddeev amplitude is reconstructed as

$$\psi(p,q;\beta|E_B)=g(p;\beta)\tau(E_B-q^2;\beta)\phi(q;\beta)G_0(E_B)\,, \tag{50}$$

where G_0 denotes the bound state propagator. Since $E_B\sim-8$ MeV $<E_{deut}$ both W and τ are free of singularities and Eq. (48) can be solved by direct matrix inversion.

In Table IV we present the trinucleon binding energies obtained with the UPE method applied to the MT I-III local *s*-wave potential. Results are listed for UPE combinations with at most two eigenvalues with an equal sign in each spin channel. We have also considered the value $s=0$ MeV in the spin singlet channel. The most pronounced jump occurs when the largest negative eigenval-

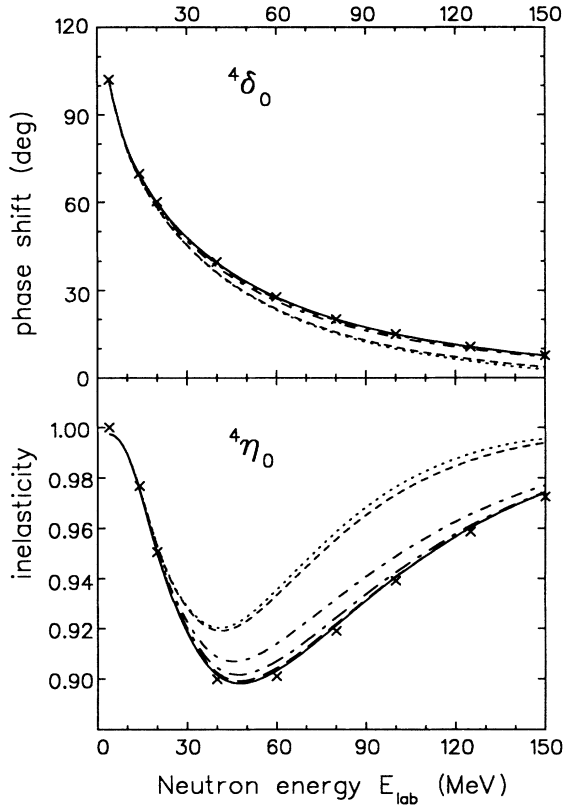

FIG. 8. *Nd* phase shift $^4\delta_0$ and inelasticity $^4\eta_0$. Again crosses refer to the local results. The meaning of the curves is as follows: (solid)=(53), (long-dashed)=(43), (long-dashed–dotted) =(33), (dashed-dotted)=(22), (dotted)=(11), (short-dashed)=UPA.

ue in the spin singlet channel is retained. Further increase of the number of eigenvalues at most accounts for a small additional decrease of the binding.

Our UPA result with $s=0$ in the $^1S_0$ channel is in agreement with the value -8.464 MeV quoted by Harms,[22] but in contrast to the value of -8.63 MeV obtained by Bakker and Ruig.[23] The accurate value for the binding energy, $E_T=-8.536$ MeV, obtained for the local MT potential is quoted from Ref. 25. In agreement with this value is the binding energy we found in determining the local trinucleon wave function. Its value is $E_T=-8.50$ MeV.

The completely antisymmetrized trinucleon bound state can easily be obtained from the Faddeev amplitudes, which already have the proper subsystem symmetry. A projection on plane wave states Eq. (A8) yields

$$\langle\psi_T|=\sum_{\beta=1}^{4}\int d\mathbf{p}_1 d\mathbf{q}_1\langle\psi_T|\mathbf{p}_1\mathbf{q}_1\beta\rangle_{1\,1}\langle\mathbf{p}_1\mathbf{q}_1\beta| \ . \tag{51}$$

The wave function coefficients are

$$\langle\psi_T|\mathbf{p}_1\mathbf{q}_1\beta\rangle_1=\langle\psi|e+P_{231}+P_{312}|\mathbf{p}_1\mathbf{q}_1\beta\rangle_1 \ , \tag{52}$$

where the state $\langle\psi|$ corresponds to the Faddeev amplitude in Eq. (50), after replacing E_B by E_T. For the $L=0$ amplitude we obtain

$$\langle\psi_T|\mathbf{p}_1\mathbf{q}_1\beta\rangle_1=\sum_{\beta'=1}^{2}\sum_{n=1}^{3}\psi(p_n,q_n;\beta')_n\langle\beta'|\beta\rangle_1 \ , \tag{53}$$

where $(\mathbf{p}_n,\mathbf{q}_n)$ are the associated momenta of $(\mathbf{p}_1,\mathbf{q}_1)$. Again our preference for particle 1 as the spectator is expressed in the choice of basis states. Substituting the values for the recoupling coefficients, we obtain the explicit form of the various trinucleon wave function components

$$\begin{aligned}
\langle\psi_T|\chi_t\eta_s\rangle_1&=\phi_t(1)+\tfrac{1}{4}\phi_t(2)-\tfrac{3}{4}\phi_s(2)\\
&\quad+\tfrac{1}{4}\phi_t(3)-\tfrac{3}{4}\phi_s(3) \ ,\\
\langle\psi_T|\chi_s\eta_t\rangle_1&=\phi_s(1)+\tfrac{1}{4}\phi_s(2)-\tfrac{3}{4}\phi_t(2)\\
&\quad+\tfrac{1}{4}\phi_s(3)-\tfrac{3}{4}\phi_t(3) \ ,\\
\langle\psi_T|\chi_s\eta_s\rangle_1&=\tfrac{1}{4}\sqrt{3}[\phi_s(2)+\phi_t(2)]\\
&\quad-\tfrac{1}{4}\sqrt{3}[\phi_s(3)+\phi_t(3)] \ ,\\
\langle\psi_T|\chi_t\eta_t\rangle_1&=-\tfrac{1}{4}\sqrt{3}[\phi_s(2)+\phi_t(2)]\\
&\quad+\tfrac{1}{4}\sqrt{3}[\phi_s(3)+\phi_t(3)] \ ,
\end{aligned} \tag{54}$$

where $\phi_m(n)$ is the Faddeev amplitude from Eq. (50) with momenta (p_n,q_n) and pair channel spin index $m=t$ or s.

The normalization of the trinucleon state is according to

$$\langle\psi_T|\psi_T\rangle=\sum_{\beta_T=1}^{4}\int d\mathbf{p}\,d\mathbf{q}|\psi_T(\mathbf{p},\mathbf{q};\beta_T)|^2=1 \ . \tag{55}$$

TABLE IV. Trinucleon binding energies in UPE. The local value is taken from Ref. 25.

UPE	$s\,^1S_0=E_d$	$s\,^1S_0=0$	UPE	$s\,^1S_0=E_d$	$s\,^1S_0=0$
1010	−8.859	−8.487	2010	−8.889	−8.512
			1020	−8.875	−8.583
1011	−8.507	−8.369	2110	−8.868	−8.493
1110	−8.838	−8.466	1021	−8.526	−8.460
1111	−8.492	−8.355	2121	−8.546	−8.479
			2222	−8.504	−8.459
Local		−8.536			

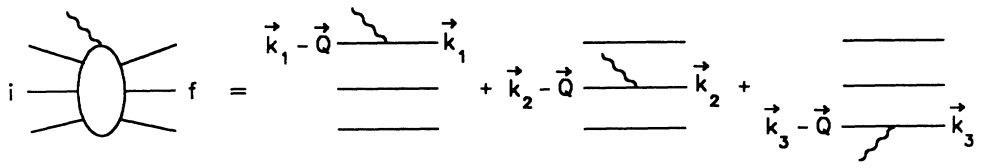

FIG. 9. Electromagnetic interaction.

IV. ELECTRON-INDUCED TWO-BODY BREAKUP

This section presents a detailed analysis of the electron induced two-body breakup reaction of ^{3}He. Non-nucleonic degrees of freedom are not considered and the NN interaction is restricted to the s-wave channel. Three-body dynamics is exactly treated in an essentially nonrelativistic description. All calculations are carried out in the lab frame, i.e., the target rest frame. Since the nuclear dynamics is treated nonrelativistically its structure only depends on the relative three-body coordinates introduced in Appendix A. However the electromagnetic current elements discussed in Sec. II need evaluation in the lab frame. Furthermore, at the considered values of energy-momentum transfer, it is preferable to employ relativistic kinematics.

To connect all these prescriptions essentially one formula is needed. Due to momentum-energy conservation the total relative kinetic energy available in a final state of three free nucleons is given by

$$s_{\text{c.m.}} = \sqrt{(\omega + M_T)^2 - \mathbf{Q}^2} - 3M_N \ , \tag{56}$$

where $q_\mu = (\mathbf{Q}; i\omega)$ is the transferred four-momentum. M_N and M_T, respectively, denote the masses of the nucleon and the trinucleon bound state system. To describe the two-body breakup process we introduce the relative nucleon-deuteron kinetic energy

$$T_{Nd} = s_{\text{c.m.}} - M_d + 2M_N \ . \tag{57}$$

M_d and M_T are taken as $2M_N + E_d$ and $3M_N + E_T$, where the binding energies E_d and E_T result from nonrelativistic calculations. The kinetic energy $s_{\text{c.m.}}$ is the on shell point in the three-nucleon scattering analysis. The energy T_{Nd} is related to the momentum q_f according to

$$T_{Nd} = q_f^2 \ , \tag{58}$$

where q_f denotes the final-state spectator momentum determining the scattering wave function in Eq. (39). The lab frame momentum p'_N of the detected nucleon follows from energy-momentum conservation

$$\omega + M_A = \sqrt{\mathbf{p}'^2_N + M_N^2} + \sqrt{(\mathbf{Q} - \mathbf{p}'_N)^2 + M_d^2} \ , \tag{59}$$

where the angle

$$\cos\gamma = x_{\text{lab}} = \hat{\mathbf{Q}} \cdot \hat{\mathbf{p}}'_N \tag{60}$$

is determined by the position of the experimental detection apparatus. Finally, the relative angle x_f is determined from the right-hand side of Eq. (A3). It should be noted that the three relations in Eqs. (56), (59), and (60) are not completely consistent with Eqs. (A3) and (A4). Fortunately, the difference due to mixing relativistic and nonrelativistic kinematics is quite small for values of the momentum transfer below 1 GeV/c.

If

$$\omega < \sqrt{[\mathbf{Q}^2 + (M_N + M_d)^2]} - M_T \ ,$$

the energy transfer is not sufficient to account for the center of mass motion and the breakup process is not allowed. Two additional restrictions $Q > \omega$ and $Q + \omega < 2E_e$ are set by the ultrarelativistic treatment of electronscattering. When

$$Q > \frac{1}{2M_N}[(T_{Nd}^2 + 2T_{Nd}(M_N + M_d) + 2M_N M_d)^2 - (2M_N M_d)^2]^{1/2} \ ,$$

a region in phase space is entered where two p'_N values satisfy Eq. (59) in the forward cone of the angle γ. Outside these regions each value of γ corresponds to one value of the momentum p'_N.

For the trinucleon system the electromagnetic current operator takes the diagrammatic form as shown in Fig. 9. The relevant nuclear current matrix element is obtained by evaluating the current operator between the initial trinucleon bound state and the final Nd scattering state. In the actual calculations we do not need a manifestly antisymmetrized final-state wave function. Since the bound state is antisymmetrized and the electromagnetic operator is symmetric in the nucleon number, we only need one of the three final-state components:

$$\frac{1}{\sqrt{3}}(|d\mathbf{q}_f\rangle_1^A + |d\mathbf{q}_f\rangle_2^A + |d\mathbf{q}_f\rangle_3^A) \to \sqrt{3}(|d\mathbf{q}_f\rangle_1^A) \ . \tag{61}$$

Here the upper index A refers to the proper symmetry in the subsystem indicated by the lower index. The factor $\sqrt{3}$ reflects the asymptotic normalization. The various diagrammatic contributions are shown in Fig. 10. Set a

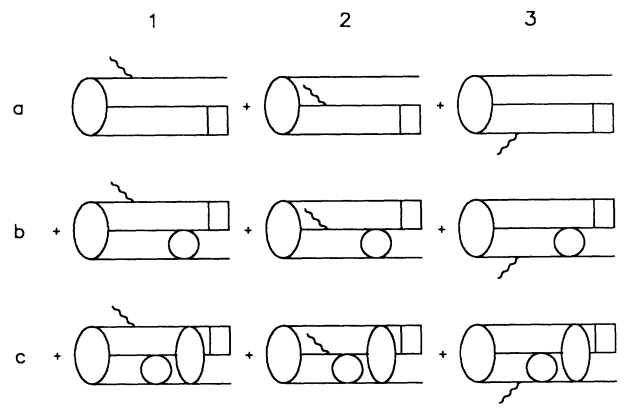

FIG. 10. Electromagnetic two-body breakup diagrams.

represents the disconnected amplitudes, set b the connected rescattering amplitudes, and set c the entire multiple scattering series amplitudes. Set b is included in c. Let us discuss these sets of diagrams and their contributions to the electromagnetic breakup cross section.

A. Born analysis

In the well-known plane wave impulse approximation (PWIA) the analysis of the breakup reaction is restricted to diagram 1a of Fig. 10. For this single amplitude the nuclear structure and the electromagnetic structure decouple, and consequently the cross section factorizes. It is convenient to express the PWIA cross section in terms of the nuclear spectral function, which general concept is introduced by Gross and Lipperheide.[26] Applied to the trinucleon system the spectral function becomes

$$S(\mathbf{p}_m,E_m;t_1^z,T_T^z)=\frac{3}{2}\sum_{J_T^z}\sum_{f\sigma_1^z}|\langle\psi_T J_T^z T_T^z|\psi_{23}f;\mathbf{p}_m\sigma_1^z t_1^z\rangle_1|^2 \times\delta[E_m-e_{23}(f)+E_T]\ . \tag{62}$$

It measures the probability to find a nucleon t_1^z with momentum $\mathbf{p}_m$ in the nucleus T_T^z leaving the residual subsystem in any state with intrinsic energy $e_{23}(f)$. The missing energy E_m is already introduced in Sec. II. Equivalently $\mathbf{p}_m$ is called the missing momentum. If the target nucleus is at rest, the missing momentum $\mathbf{p}_m$ is related to the recoil momentum $\mathbf{p}_{\rm rec}$ of the residual nucleus according to $\mathbf{p}_m=-\mathbf{p}_{\rm rec}$. The dummy index f labels all the remaining quantum numbers of the residual nucleus. Due to the rotational invariance of both the target nucleus and the residual nucleus, the spectral function S depends only on the length of the momentum $\mathbf{p}_m$. Therefore, the missing momentum and the recoil momentum are equivalent quantities in evaluating the spectral function. For an extensive treatment of the spectral function S including sum rule properties we refer to Hajduk and Sauer.[6]

In two-body breakup, which is well separated from three-body breakup by the missing energy, it is customary to introduce the momentum distribution ρ_2, which can be extracted from the spectral function after a trivial integration over the missing energy up to $-E_T$,

$$\rho_2(\mathbf{p}_m;t_1^z=T_T^z)=\tfrac{3}{2}\sum_{J_T^z}\sum_{j_d^z\sigma_1^z}|\langle\psi_T J_T^z T_T^z|\phi_d j_d^z;\mathbf{p}_m\sigma_1^z t_1^z\rangle_1|^2\ . \tag{63}$$

In terms of the s-wave triton and deuteron wave functions, expressed in Eqs. (53) and (B4), the momentum distribution reduces to

$$\rho_2(\mathbf{q}_m;T_T^z)=3\left|\int d\mathbf{p}_1\psi_T(\mathbf{p}_1\mathbf{q}_m;\beta=\chi_t^d\eta_s^d)\phi_d(\mathbf{p}_1)\right|^2\ , \tag{64}$$

where $\mathbf{q}_m=-\frac{1}{2}\sqrt{3/M_N}\mathbf{p}_m$. Results for the momentum distribution ρ_2 are shown in Fig. 11. Already the UPA calculation leads to a very reasonable reproduction of the momentum distribution obtained with the local MT potential, while the convergence of the (2222)-UPE separable term is almost excellent. Evidently the constructing amplitude changes sign at a missing momentum of about 450 MeV/c. It reflects the presence of a repulsive component in the MT interaction. To show this we have also plotted the ρ_2 result for a Yamaguchi-type interaction, which is purely attractive. (Parameters are taken from Ref. 13.) In that case the amplitude has a definite sign in the entire momentum interval. The ρ_2 value at zero missing momentum is directly related to the trinucleon binding energy, which appears in the wave function propagator. The much lower Yamaguchi starting point is due to an unrealistically strong binding of -11.0 MeV.

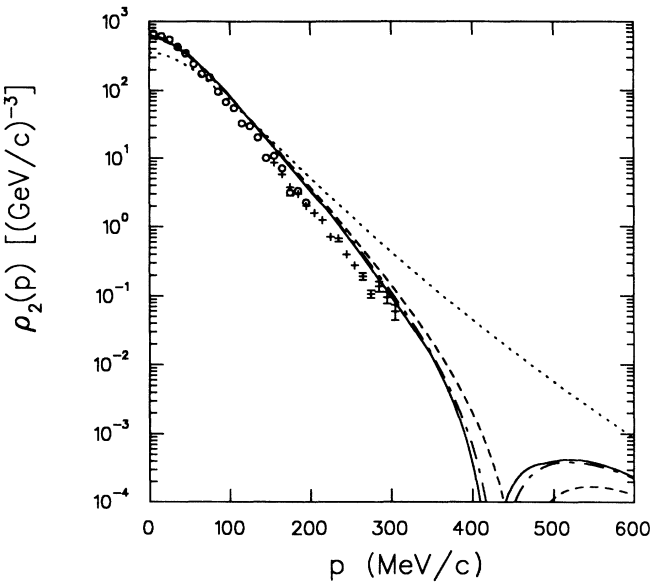

FIG. 11. Momentum distribution function ρ_2. The solid curve is calculated with the local MT interaction. The dashed and long-dashed–dotted curves result from an UPA and a (2222)-UPE calculation. The dotted curve is due to a Yamaguchi form factor. The data points are due to Jans (Ref. 2). They are extracted from $(e,e'p)$ measurements assuming the validity of PWIA.

Thus, the PWIA contribution is directly proportional to the ρ_2 momentum distribution sampled at $p_m=|\mathbf{p}'_N-\mathbf{Q}|$. The electromagnetic interaction is expressed into the half-off-shell electron-nucleon cross section σ_{eN} presented in Sec. II and consequently we can write the threefold PWIA cross section as

$$\frac{d^3\sigma}{d\Omega_{e'}dE_{e'}d\Omega_{p'_N}}=k_f\sigma_{eN}\rho_2(|\mathbf{p}'_N-\mathbf{Q}|;T_T^z)\ . \tag{65}$$

where the kinematic factor k_f is given by

$$k_f=\int dE_{p'_N}\frac{\partial p'_N}{\partial E_{p'_N}}p'^2_N\delta[\omega+M_T-\sqrt{p'^2_N+M_N^2}-\sqrt{(\mathbf{Q}-\mathbf{p}'_N)^2+M_d^2}] =p'_N E_{p'_N}\left[1-\left[\frac{\mathbf{Q}\cdot\hat{\mathbf{p}}'_N-p'_N}{p'_N}\right]\frac{E_{p'_N}}{E'_d}\right]^{-1}\ , \tag{66}$$

with E_d' the lab energy of the knocked out deuteron.

The factorization of the nuclear and electromagnetic structure as found for PWIA is not valid for the remaining diagrams 2*a*, 3*a*, and *b* and *c* in Fig. 10. The complete two-body breakup amplitude of the trinucleon system with only nucleonic degrees of freedom for the nuclear current and nuclear wave functions constructed from *s*-wave *NN* interactions is expressed as

$$A_\mu^\lambda(d,\mathbf{q}_f;\beta_f)=\sqrt{3}\sum_{n=1}^{3}\sum_{\beta_T=1}^{4}\sum_{\beta_1=1}^{3}\int d\mathbf{p}_1 d\mathbf{q}_1 \psi_T(\mathbf{p}_1^{(n)},\mathbf{q}_1^{(n)};\beta_T) S_\mu^\lambda[\mathbf{k}_n(\mathbf{p}_1,\mathbf{q}_1),\sigma_n,t_n^z;\beta_T,\beta_1] f(\mathbf{p}_1,\mathbf{q}_1;\beta_1|d,\mathbf{q}_f;\beta_f) . \quad (67)$$

The trinucleon wave function ψ_T and final-state wave function f are given by the Eqs. (54) and (39). The functions S_μ^λ contain the nucleon current elements and are closely related to the quantities S or $\bar{S}$ expressed in Eqs. (28) and (30),

$$S_\mu^\lambda[\mathbf{k}_n(\mathbf{p}_1,\mathbf{q}_1),\sigma_n,t_n^z;\beta_T,\beta_1] = {}_1\langle \mathbf{p}_1^{(n)}\mathbf{q}_1^{(n)}\beta_T | j_\mu^\lambda(k_n,\sigma_n,t_n^z)|\mathbf{p}_1\mathbf{q}_1\beta_1\rangle_1 . \quad (68)$$

The only relevant modification is that the functions S_μ^λ require evaluation in three-nucleon Hilbert space. The momentum of the active nucleon in the lab frame just after the electromagnetic interaction is denoted by the variable $\mathbf{k}_n$. It depends on the Jacobi coordinates $\mathbf{p}_1$ and $\mathbf{q}_1$ according to Eqs. (A3) and (A4). The spin-isospin structure of Eq. (68) is treated in Appendix D.

The indices on the amplitude A denote the component of the nuclear current (μ) and the component of the Pauli spin matrix (λ) [see Eq. (26)]. Since the deuteron is isospin zero the possible final spin-isospin channels (β_f) are $|\chi_t^d\eta_s\rangle$ and $|\chi_t^q\eta_s\rangle$ in the notation of Eqs. (A16)–(A18).

Taking the momenta $(\mathbf{p}_1,\mathbf{q}_1)$ as integration variables is advantageous for several reasons. In this way the momentum transfer $\mathbf{Q}$ is only present in the ground state, via the momenta $\mathbf{p}_1^{(n)}$ and $\mathbf{q}_1^{(n)}$, and in the electromagnetic current; the final state does not depend on $\mathbf{Q}$. Furthermore, since we only need one final-state component [Eq. (61)] the diagrams can be arranged in such a way that the nucleons labeled 2 and 3 are involved in the first strong interaction after the electromagnetic interaction. This part depends only on the momentum $\mathbf{p}_1$. From Eq. (47) we see that the complicated spectator wave function for the connected part, Eq. (45), can be completely kept outside the $\mathbf{p}_1$ integration. Of course, this property is only valid for separable potentials. In case of a central local potential the above statement is restricted to the Ω_{p_1} integration. Finally, the free propagator G_0 in the final state depends only on p_1 and q_1, and not on the angles. This implies that subtraction techniques can be used straightforwardly to integrate the physical pole.

Before turning to a detailed treatment of the various amplitudes, we first discuss the structure of the momentum dependence of the amplitude in Eq. (67). The bound state momenta $(\mathbf{p}_1^{(n)},\mathbf{q}_1^{(n)})$ are related to $(\mathbf{p}_1,\mathbf{q}_1)$ via the momentum transfer $\mathbf{Q}_m=\mathbf{Q}/\sqrt{3M}$ on nucleon n. In terms of the matrix α_{ji} introduced in Eq. (A14), we have

$$\begin{bmatrix}\mathbf{p}_1^{(n)}\\ \mathbf{q}_1^{(n)}\end{bmatrix}=\begin{bmatrix}\mathbf{p}_1\\ \mathbf{q}_1\end{bmatrix}+\alpha_{ji}^{1-n}\begin{bmatrix}0\\ \mathbf{Q}_m\end{bmatrix} . \quad (69)$$

The bound state exchange momenta $(\mathbf{p}_2^{(n)},\mathbf{q}_2^{(n)})$ and $(\mathbf{p}_3^{(n)},\mathbf{q}_3^{(n)})$ are obtained from $(\mathbf{p}_1^{(n)},\mathbf{q}_1^{(n)})$ by an additional operation α_{21}, respectively, $\alpha_{31}=\alpha_{21}^{-1}$. The contributions from $n=2$ and $n=3$ can be taken together in the $\mathbf{p}_1$ integration, as is shown hereafter. From the properties of the matrix α_{ji} it follows immediately that

$$\begin{aligned}\mathbf{p}_2^{(3)}(\mathbf{p}_1,\mathbf{q}_1)&=\mathbf{p}_3^{(2)}(-\mathbf{p}_1,\mathbf{q}_1) ,\\ \mathbf{q}_2^{(3)}(\mathbf{p}_1,\mathbf{q}_1)&=\mathbf{q}_3^{(2)}(\mathbf{p}_1,\mathbf{q}_1)\end{aligned} \quad (70)$$

and

$$\begin{aligned}\mathbf{p}_1^{(3)}(\mathbf{p}_1,\mathbf{q}_1)&=\mathbf{p}_1^{(2)}(-\mathbf{p}_1,\mathbf{q}_1) ,\\ \mathbf{q}_1^{(3)}(\mathbf{p}_1,\mathbf{q}_1)&=\mathbf{q}_1^{(2)}(\mathbf{p}_1,\mathbf{q}_1) .\end{aligned}$$

The momentum dependence of the nucleon current is contained in $S_\mu^\lambda[\mathbf{k}_n(\mathbf{p}_1,\mathbf{q}_1,\mathbf{Q})]$. Due to Eqs. (A3) and (A4) we have

$$\mathbf{k}_3(\mathbf{p}_1,\mathbf{q}_1,\mathbf{Q})=\mathbf{k}_2(-\mathbf{p}_1,\mathbf{q}_1,\mathbf{Q}) . \quad (71)$$

Since the final-state wave function only depends on the length of $\mathbf{p}_1$ we find that the substitution $\mathbf{p}_1\rightarrow-\mathbf{p}_1$ interchanges the set of diagrams 2↔3 in Fig. 10, at least with respect to the momentum dependence. For the bound state components with odd spin-isospin parity this correspondence is exact, however in the even channels the substitution induces an additional minus sign.

We now evaluate the disconnected Born-type diagrams *a* from Fig. 10. In relation to the momentum distribution expressed in Eq. (64) the PWIA amplitude simply becomes

$$A_\mu^{\lambda(\mathrm{PWIA})}(d,\mathbf{q}_f;\beta_f)=S_\mu^\lambda[\mathbf{k}_1(\mathbf{q}_f,\mathbf{Q}),\sigma_1,t_1^z;\beta_T=\chi_t\eta_s,\beta_f]\sqrt{3}\int d\mathbf{p}_1\psi_T(\mathbf{p}_1^{(1)},\mathbf{q}_1^{(1)};\beta_T=\chi_t\eta_s)\phi_d(\mathbf{p}_1) . \quad (72)$$

Also in the disconnected diagrams 2*a* and 3*a* of Fig. 10, the spectator wave function $\delta(\mathbf{q}_1-\mathbf{q}_f)$ is trivially removed. However the electromagnetic interaction cannot be extracted from the integration, and the contributing Born-type amplitude becomes

$$A_\mu^{\lambda(\mathrm{DDKO})}(d,\mathbf{q}_f;\beta_f)=\sqrt{3}\sum_{n=2}^{3}\sum_{\beta_T=1}^{4}\int d\mathbf{p}_1\psi_T(\mathbf{p}_1^{(n)},\mathbf{q}_1^{(n)};\beta_T)S_\mu^\lambda[\mathbf{k}_n(\mathbf{p}_1,\mathbf{q}_f,\mathbf{Q}),\sigma_n,t_n^z;\beta_T,\beta_f]\phi_d(\mathbf{p}_1) , \quad (73)$$

where DDKO stands for direct deuteron knockout. To make use of the similar momentum dependence of the components $n=2$ and $n=3$ we rearrange the various current combinations with respect to the spin-isospin structure of the pair (2,3). Before doing so we discuss the structure of the elements S_μ^λ in more detail. The spin dependence is given by

$$S_\mu = S_\mu^0 + i\mathbf{S}_\mu \boldsymbol{\sigma} \ , \tag{74}$$

while every element S_μ^λ can be decomposed into an isoscalar and isovector part

$$S = S_S + S_V \tau^z \ . \tag{75}$$

In terms of a set of new components, defined as

$$S_{\mu(\pm)}^\lambda = S_{\mu(2)}^\lambda \pm S_{\mu(3)}^\lambda, \quad \boldsymbol{\sigma}_{(\pm)} = \tfrac{1}{2}(\boldsymbol{\sigma}_{(2)} \pm \boldsymbol{\sigma}_{(3)}), \quad \tau_{(\pm)}^z = \tfrac{1}{2}(\tau_{(2)}^z \pm \tau_{(3)}^z) \ , \tag{76}$$

we obtain for the spin-independent combination

$$S^0(2) + S_{(3)}^0 = S_{S(+)}^0 + S_{V(+)}^0 \tau_{(+)}^z + S_{V(-)}^0 \tau_{(-)}^z \ . \tag{77}$$

Similarly we get for the spin-dependent component

$$\begin{aligned} \mathbf{S}_{(2)} \cdot \boldsymbol{\sigma}_{(2)} + \mathbf{S}_{(3)} \cdot \boldsymbol{\sigma}_{(3)} = {} & \mathbf{S}_{S(+)} \cdot \boldsymbol{\sigma}_{(+)} + \mathbf{S}_{S(-)} \cdot \boldsymbol{\sigma}_{(-)} + \mathbf{S}_{V(+)} \cdot \boldsymbol{\sigma}_{(+)} \tau_{(+)}^z + \mathbf{S}_{V(-)} \cdot \boldsymbol{\sigma}_{(-)} \tau_{(+)}^z \\ & + \mathbf{S}_{V(+)} \cdot \boldsymbol{\sigma}_{(-)} \tau_{(-)}^z + \mathbf{S}_{V(-)} \cdot \boldsymbol{\sigma}_{(+)} \tau_{(-)}^z \ . \end{aligned} \tag{78}$$

These two equations are valid for each current component μ. We prefer to keep the index λ on the resulting amplitude A_μ^λ until we take the trace over unobserved spin states.

According to the discussion on the substitution $\mathbf{p}_1 \to -\mathbf{p}_1$ we conclude that the $S_{(+)}(S_{(-)})$ parts of the current go along with the odd, $\beta_T = 1,2$ (even, $\beta_T = 3,4$) spin-isospin components of the triton. With this restriction in mind we can replace $\sum_{n=2}^3$ in Eq. (73) by $2\sum_{n=2}^2$. The (iso)spin structure of the matrix elements take the form ${}_1\langle \chi^{(i)} | \boldsymbol{\sigma}_{(\pm)} | \chi^{(f)} \rangle_1$ and ${}_1\langle \eta^{(i)} | \tau_{(\pm)}^z | \eta^{(f)} \rangle_1$, where $f(i)$ labels the final (initial) state. Since we do not prepare nor observe polarization degrees of freedom we can restrict the spin analysis to one component due to rotational invariance in Pauli spinor space and the absence of spin-orbit coupling in the nuclear dynamics. In Appendix D we have collected the values of the relevant coefficients for the z component.

Apart from the specific values of these matrix elements, we note that the $(\tau_{(+)})\sigma_{(+)}$ elements conserve the pair (iso)spin, whereas the $(\tau_{(-)})\sigma_{(-)}$ elements induce an (iso)spin flip in the subsystem (2,3). In the DDKO process the initial $(\chi_s \eta_t)$ state couples through the $\mathbf{S}_{V(+)} \cdot \boldsymbol{\sigma}_{(-)} \tau_{(-)}^z$ term to the deuteron final state. In presenting the results in the accompanying paper[27] we will show that this contribution is considerable. In most kinematic situations the $S_{(-)}$ induced contributions are small compared to the $S_{(+)}$ contributions, generally of the order of 1%. This is due to the small contributions from the even bound state components.

The momentum integration for the DDKO diagram is straightforward. There are no singularities, since the spectator momentum is fixed at $q_f^2 = s_{\text{c.m.}} - E_d$. The azimuthal integration can be restated as $2\int_{\phi q_f}^{\phi q_f + \pi} d\phi_p$. The polar-angle integration $\int_{-1}^{+1} d\cos\theta_p$ is just done as it stands, and the radial integration $\int dp\, p^2 \cdots$ is performed after mapping a Gauss-Legendre quadrature from $[0,1] \to [0,\infty]$ according to

$$p \leftarrow c_p \ln \frac{1+p}{1-p} \ . \tag{79}$$

B. Connected graph contributions

Using Eqs. (47) and (67) we find that the connected contribution can be written as

$$\begin{aligned} A_\mu^{\lambda(\text{FSI})}(d, \mathbf{q}_f; \beta_f) = -\sqrt{3} \sum_{n=1}^{3} \sum_{\beta_T=1}^{4} \sum_{\beta_1=1}^{3} \int d\mathbf{p}_1 d\mathbf{q}_1 \psi_T(\mathbf{p}_1^{(n)}, \mathbf{q}_1^{(n)}; \beta_T) S_\mu^\lambda[\mathbf{k}_n(\mathbf{p}_1, \mathbf{q}_1, \mathbf{Q}), \sigma_n, t_n^z; \beta_T, \beta_1] \\ \times \frac{1}{p_1^2 + q_1^2 - s_{\text{c.m.}} - i\varepsilon} g(p_1; \beta_1) \tau(s_{\text{c.m.}} - q_1^2; \beta_1) \\ \times \sum_{l=0}^{L_{\max}} (2l+1) P_l(\hat{\mathbf{q}}_1 \cdot \hat{\mathbf{q}}_f) \psi_l^{\text{Padé}}(q_1; \beta_1 | q_f; \beta_f) \ . \end{aligned} \tag{80}$$

The index Padé refers to the way the scattering state is constructed. For the cutoff partial wave number we took $L_{\max} = 10$, which is on the safe side of the optimal choice.

The numerical integration turns out to be fivefold since the azimuthal ϕ_{q_1} integral can be carried out analytically, provided we treat the current contributions in S_μ^λ separately with respect to both indices λ and μ. Due to rotational invariance of the trinucleon wave function the relevant ϕ_{q_1} dependence of the various terms in the integrand has the form

$$\int_0^{2\pi} d\phi_{q_1} P_l(\hat{\mathbf{q}}_1\cdot\hat{\mathbf{q}}_f) f(\phi_{q_1}) \tag{81}$$

with $f(\phi)=1$, $\cos\phi$, $\sin\phi$, $\cos 2\phi$, or $\sin 2\phi$, after the integral over the azimuthal angle ϕ_{p_1} is performed according to $\int_{\phi q_1}^{2\pi+\phi_{q_1}} d\phi_{p_1}$. Using the well-known relation[28]

$$P_l(\hat{\mathbf{q}}_1\cdot\hat{\mathbf{q}}_f)=P_l(x_{q_1})P_l(x_{q_f}) + 2\sum_{m=1}^{l}\frac{(l-m)!}{(l+m)!}P_l^m(x_{q_1})P_l^m(x_{q_f}) \times\cos[m(\phi_{q_1}-\phi_{q_f})] , \tag{82}$$

where $x_{q_1}=\hat{\mathbf{q}}_1\cdot\hat{\mathbf{Q}}$ and $x_{q_f}=\hat{\mathbf{q}}_f\cdot\hat{\mathbf{Q}}$, these integrals can be done explicitly. Since $\phi_{q_f}=\pi$ by definition, the contributions coming from the sin terms in Eq. (81) drop out.

Substituting Eq. (82) into Eq. (80), we find that for each partial wave component l and for each current component λ,μ the x_{q_f} dependence factorizes in terms of one specific P_l^m function and can be separated from the remaining part of the expression. It implies that for a specific (Q,ω) point in kinematic phase space, the integrals for the connected diagram need to be performed only one time in order to calculate the cross section as a function of the third independent kinematic parameter, $\cos\theta_{q_f}=\hat{\mathbf{q}}_f\cdot\hat{\mathbf{Q}}$.

The polar integrals $\int d\cos\theta_{p_1}$ and $\int d\cos\theta_{q_1}$ are carried out straightforwardly using 8- and 12-point Gauss-Legendre quadratures, respectively. The singularity in the propagator is removed in the radial p_1 integration by means of a subtraction technique. The same technique is used to account for the pole of the two-particle propagator at the deuteron point. The presence of the complicated q-dependent logarithmic structure like in the construction of the scattering wave function is avoided due to the proper choice of integration variables and the use of plane wave states rather than angular momentum states. The threshold point of the three-particle sector shows up as an inverse square root singularity $(s_{\text{c.m.}}-q_1^2)^{-1/2}$, but this pole is integrable.

In Sec. III we have discussed the convergence rate of some UPE observables with respect to the original local interaction. The momentum distribution ρ_2 for the local MT interaction is shown in Fig. 11, together with the results for the separable expansion. Similarly, we have extended the analysis of the two-body breakup process to local interactions in order to study the UPE convergence property for the electromagnetic process. To calculate the off-shell two-body T matrix we have used the Kowalski and Noyes[29] procedure. Technical details can be found in Ref. 13. Once the off-shell two-body T matrix elements for energies below $s_{\text{c.m.}}$ are known, the three-nucleon functions can be computed. In the three-body sector no conceptual difficulties arise in turning to a local interaction and the equations can be solved along the same lines. Only the numerical effort required increases drastically. In view of this the UPA might be regarded as a very useful tool for testing purposes.

Subsequently, the electromagnetic breakup process is computed in precisely the same way as outlined before. Two modifications are needed. The p_1 integration must be reorganized, since the final-state wave function is already present there. Furthermore, since the (p_1,q_1) integration mesh does not necessarily coincide with the (p,q) grid on which the wave functions are determined we have to apply an interpolation procedure. The Faddeev bound state amplitude is a smooth and rather unstructered object in both variables. A bicubic interpolation routine is sufficiently accurate. The same applies to the Faddeev scattering amplitude except for the square root cusp at $q^2=s_{\text{c.m.}}$ and the deuteron pole at $q^2=s_{\text{c.m.}}-E_d$ in the spectator momentum dependence, but this structure was already encountered in the UPE analysis. The numerical implementation of the above mentioned modifications is checked to be correct by means of a calculation with two-dimensional wave functions reconstructed from the factorized UPA components.

C. Nuclear structure functions

The full amplitude is found by summing the disconnected and connected amplitudes

$$A_\mu^\lambda(d,\mathbf{q}_f;\beta_f)=A_\mu^{\lambda(\text{PWIA})}+A_\mu^{\lambda(\text{DDKO})}+A_\mu^{\lambda(\text{FSI})} . \tag{83}$$

To obtain the nuclear structure functions

$$W_j(Q,\omega,p_N',\theta_{p_N'}) \quad j=CTSI , \tag{84}$$

such as defined in Eq. (14), we have to sum over the unobserved final spin-isospin states $|\beta_f\rangle$. Furthermore we remove the index λ by taking the trace in two-component spinor space. Thus, the nuclear structure functions can be obtained from

$$\begin{aligned} W_C&=\Sigma_{\beta_f}(|A_\rho^0|^2+|\mathbf{A}_\rho|^2) ,\\ W_T&=2\Sigma_{\beta_f}(|A_\perp^0|^2+|\mathbf{A}_\perp|^2) ,\\ W_S&=\Sigma_{\beta_f}(|A_\parallel^0|^2-|\mathbf{A}_\perp^0|^2)+\Sigma_{\beta_f}(|\mathbf{A}_\parallel|^2-|\mathbf{A}_\perp|^2) ,\\ W_I&=-\Sigma_{\beta_f}(A_\rho^{*0}A_\parallel^0+\mathbf{A}_\rho^*\cdot\mathbf{A}_\parallel) -\Sigma_{\beta_f}(A_\parallel^{*0}A_\rho^0+\mathbf{A}_\parallel^*\cdot\mathbf{A}_\rho) , \end{aligned} \tag{85}$$

where we have omitted the energy conserving delta function. The threefold two-body breakup cross section is given by

$$\frac{d^3\sigma}{d\Omega_{e'}dE_{e'}d\Omega_{p_N'}}=k_f\sigma_{\text{Mott}}(v_C W_C+v_T W_T +v_S W_S+v_I W_I) , \tag{86}$$

where the kinematic factor k_f corresponds to expression (66). The electron-photon factors v_j are expressed in Eq. (13). In some experiments the deuteron is detected rather than the proton and the differential cross section with respect to the angle $\Omega_{p_d'}$ is measured. In the right-hand side of (86) this amounts to a trivial modification of the kinematic factor.

As an example of an electromagnetic two-body breakup calculation we consider the Johansson experiment[30] with PWIA dominated kinematics. For other applications we refer to the accompanying paper.[27] Figure 12 presents ^{3}He$(e,e'p)d$ coincidence data taken at $E_e=550$ MeV. The data were measured and analyzed by Johansson and reanalyzed by Gibson and West.[31] The Born+FSI result is shown, together with the PWIA result. This kinematic situation has been studied by Lehman *et al.*,[11] who have carried out an exact calculation using Yamaguchi separable potentials. We have also examined this case taking the potential parameters from Ref. 13 and find qualitatively the same results. Besides the use of slightly different potential form factors, the differences found may be due to the use of nonrelativistic electromagnetic operators by Heimbach *et al.*[11] as compared to Eq. (31). For the Yamaguchi form factors we find that the cross section is reduced by about 4–7 % due to final-state effects. The small influence of FSI is not surprising, because the kinematics in this experiment were such that rather low nucleon momenta ($p_{\rm miss}<100$ MeV/c) were probed with a rather high three-momentum transfer ($Q=443$ MeV/c). In this situation the process of direct proton knockout dominates, i.e., diagram 1a in Fig. 10. The curves are not completely symmetric with respect to the point of zero missing momentum, since the nuclear structure function W_1 contributes with opposite sign in the two kinematic regions separated by the parallel point $\Theta_{p'_N e}=52°$. Figure 12 clearly shows that the UPA calculation leads to a better reproduction of the data than does a calculation with Yamaguchi form factors. In view of the momentum distribution ρ_2 (see Fig. 11) this discrepancy can be fully ascribed to the different values for the binding energies.

For this kinematic setup we have also studied the sensitivity of the UPA Born+FSI cross sections for variations of several features of the electromagnetic current input. Figure 13 displays the results, where the UPA Born+FSI curve from Fig. 12 evaluated for the relativistic current of Eq. (23) serves as a reference. We see that using the current with the more convenient $\sigma_{\mu\nu}$ term from Eq. (24) leads to an entirely equivalent result. A nonrelativistic expansion of the current up to $\mathcal{O}(1)$ or $\mathcal{O}(1/M_N^2)$ like in Eq. (31) does influence the result considerably and at the discussed values of the momentum-energy transfer such approximations clearly break down and it is important to take the full relativistic expression. Finally, in order to see what kind of off-shell sensitivity one may expect we have also considered the option of eliminating the charge component in favor of the longitudinal current in the calculation of the structure function. As is seen in Fig. 13 the calculated result is substantially lower, reflecting the sensistivity as already discussed in Sec. II.

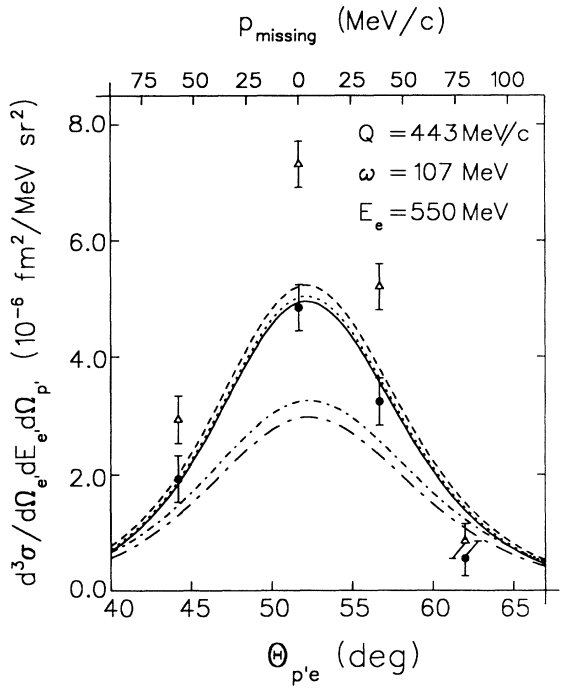

FIG. 12. Coincidence cross section for the ^{3}He$(e,e'p)d$ reaction at fixed momentum and energy transfer. The upper curves correspond to a PWIA (dashed) and Born+FSI (solid) calculation with a UPA MT potential. The dotted curve represents the Born+rescattering connected diagrams (i.e., diagrams $a+b$ in Fig. 10). The lower curves correspond to a PWIA (short-dashed–dotted) and Born+FSI (long-dashed–dotted) calculation with Yamaguchi form factors. Original data are from Ref. 30 (triangles) and reanalyzed data are from Ref. 31.

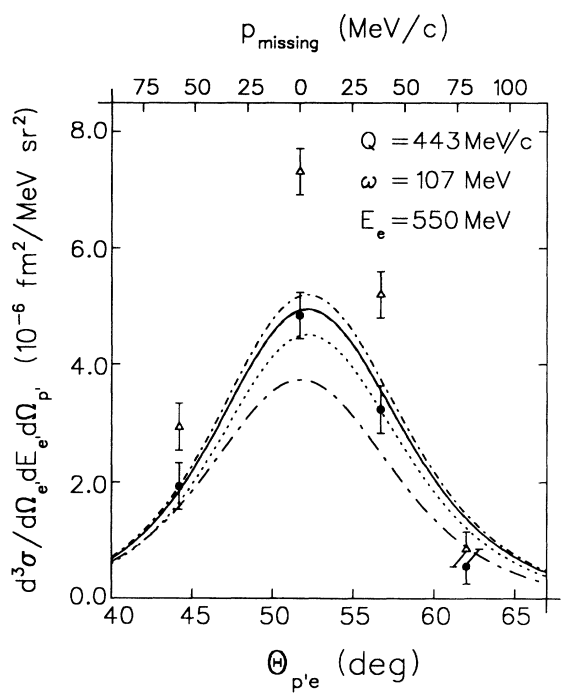

FIG. 13. Sensitivity study of various electromagnetic components in kinematic situation equivalent to Fig. 12. Data and solid line are taken from Fig. 12. The dashed line is obtained with the current from Eq. (24). The nonrelativistic current reductions are displayed by the long-dashed–dotted [$O(1)$] and short-dashed–dotted [$O(1/M_N^2)$] curves. Elimination of the charge component results in the dotted curve.

V. SUMMARY

This work provides a detailed treatment of the electromagnetic two-body breakup of ^{3}He, calculated with nucleonic final-state interactions exactly taken into account. The distortion between the outgoing nucleon and the residual nuclear system is included by solving the Faddeev equations for continuum states. The unpolarized coincidence cross section in electron scattering can be expressed in terms of four nuclear structure functions. We considered the nuclear current to be composed of one-nucleon current components only, for which we took an on-mass-shell form. Hence meson exchange currents have not been considered in this paper. Since the virtual photons are interacting with bound nucleons, these one-nucleon currents in general no longer satisfy current conservation. To comply with this the half-off-shell prescription introduced by de Forest[14] has been adopted. Sensitivity to various other *ad hoc* choices has been studied, indicating sizable variations in the momentum transfer region considered.

Although we show that it is feasible to employ a local s-wave NN interaction, the majority of two-body breakup results, which we present, is obtained with a separable interaction. In particular, we investigated the possibility to approach a realistic s-wave local potential by means of the unitary pole expansion (UPE) method. The UPE convergence properties in describing the NN and Nd scattering observables turn out to be quite satisfactory. Retaining four eigenvalues in each spin channel almost exactly reproduces the values for the observables obtained with the local interaction. An almost equally important result is that already the first-term approach (UPA) leads to a fair reproduction of the local values. This makes UPA an attractive tool for the actual numerical calculations of the electromagnetic breakup reactions of the $A=3$ system.

ACKNOWLEDGMENTS

Part of the numerical computations have been carried out on a Cyber 205. This was made possible by the Stichting Surf, the Netherlands.

APPENDIX A: NOTATION

In a nonrelativistic theory, three particles, each with spin $\frac{1}{2}$ and isospin $\frac{1}{2}$, can be represented by normalized states

$$|\mathbf{k}_1\mathbf{k}_2\mathbf{k}_3 s_1^z s_2^z s_3^z t_1^z t_2^z t_3^z\rangle \ , \tag{A1}$$

where $\mathbf{k}_i$ denotes the momentum of particle i and s_i^z, t_i^z label the spin and isospin component of particle i. The kinetic energy of this state is

$$E_0=\mathbf{k}_1^2/2M_1+\mathbf{k}_2^2/2M_2+\mathbf{k}_3^2/2M_3 \ . \tag{A2}$$

Hereafter, we only consider nucleons with equal mass M_N. To split off the center of mass motion we introduce the relative momenta

$$\begin{aligned}\mathbf{K}&=\mathbf{k}_1+\mathbf{k}_2+\mathbf{k}_3 \ ,\\ \mathbf{k}_{p_i}&=\tfrac{1}{2}(\mathbf{k}_j-\mathbf{k}_k) \ ,\\ \mathbf{k}_{q_i}&=\tfrac{1}{3}(\mathbf{k}_j+\mathbf{k}_k-2\mathbf{k}_i) \ ,\end{aligned} \tag{A3}$$

where (ijk) is a cyclic permutation of (123). It is convenient to eliminate the masses from the energy of the relative motion by introducing scaled relative momenta

$$\mathbf{p}_i=\left[\frac{1}{M_N}\right]^{1/2}\mathbf{k}_{p_i} \quad \text{and} \quad \mathbf{q}_i=\frac{1}{2}\left[\frac{3}{M_N}\right]^{1/2}\mathbf{k}_{q_i} \ . \tag{A4}$$

In this way the kinetic energy becomes

$$E_0=\frac{1}{6M_N}\mathbf{K}^2+\mathbf{p}^2+\mathbf{q}^2 \ , \tag{A5}$$

where indices on p and q would be redundant. Throughout the entire paper, we use the so-called Jacobi coordinates of Eq. (A4). If we consider only the momenta, the relevant part of Eq. (A1) becomes

$$|\mathbf{p}_i\mathbf{q}_i\rangle_i \ . \tag{A6}$$

Since there are three particles, Eq. (A6) represents three equivalent states, and as mentioned before $p_i^2+q_i^2$ does not depend on the label. It is essential to note that the indices i in Eq. (A6) have different meanings. The index on the ket $|\ \rangle$ refers to the coupling scheme adopted in Eq. (A3), i.e., first $j+k\rightarrow(jk)$ and then $(jk)+i\rightarrow(jk)i$, whereas the index on the momentum just expresses that particle i has a momentum $\mathbf{k}_i$.

Since we are dealing with identical particles, the three-nucleon wave functions must be antisymmetric with respect to a permutation operation

$$P_i^{\text{total}}=P_i^{\text{space}}P_i^{\text{spin}}P_i^{\text{isospin}} \ .$$

The operators P_i $(i=1,2,3)$, which interchange the labels of particle j and k, form the odd elements of the permutation group S_3. The even elements of S_3 are the identity e, and the operators P_{jki} and P_{kij}, which perform a cyclic shift of the arrangement (ijk). From the elements of S_3 we can construct the antisymmetrizer

$$A_3=A_{2_i}P_s \ , \tag{A7}$$

with

$$P_s=\frac{1}{\sqrt{3}}(e+P_{231}+P_{312}) \ , \tag{A8}$$

and

$$A_{2_i}=\frac{1}{\sqrt{2}}(1-P_i) \ . \tag{A9}$$

P_s antisymmetrizes a three-nucleon state that is antisymmetric in at least one pair. Such a state is constructed by A_{2_i} operating on an arbitrary three-nucleon state. The operator A_3 does not depend on the index i.

At this point, it is straightforward to introduce a new set of basis states which are antisymmetric with respect to at least one pair.

$$|\mathbf{pq}\beta\rangle_i^A = A_{2_i}|\mathbf{pq}\beta\rangle_i \ , \qquad |\alpha\mathbf{q}\beta\rangle_i^A = A_{2_i}|\alpha\mathbf{q}\beta\rangle_i \ . \tag{A10}$$

Here α labels a two-nucleon bound state and β represents all remaining spin-isospin quantum numbers. Since the basis states $|\mathbf{pq}\beta\rangle_i$ and $|\alpha\mathbf{q}\beta\rangle_i$ are normalized to "one," the partially antisymmetrized states from Eq. (A10) have the normalization

$$\begin{aligned} {}_i^A\langle \mathbf{pq}\beta|\mathbf{p'q'}\beta'\rangle_i^A &= \delta_{\beta\beta'}\delta(\mathbf{q}-\mathbf{q'}) \\ &\quad \times[\delta(\mathbf{p}-\mathbf{p'})-(-1)^{\beta_p}\delta(\mathbf{p}+\mathbf{p'})] \ , \\ {}_i^A\langle \alpha\mathbf{q}\beta|\alpha\mathbf{q'}\beta'\rangle_i^A &= 2\delta_{\beta\beta'}\delta(\mathbf{q}-\mathbf{q'})\delta'_{\alpha\alpha} \ . \end{aligned} \tag{A11}$$

The effective closure relations are

$$\mathbf{I} = \sum_\beta \int d\mathbf{p}\, d\mathbf{q}\, |\mathbf{pq}\beta\rangle_{i\,i}\langle \mathbf{pq}\beta| \ , \qquad \mathbf{I} = \tfrac{1}{2}\sum_\beta \int d\mathbf{p}\, d\mathbf{q}\, |\mathbf{pq}\beta\rangle_i^A {}_i^A\langle \mathbf{pq}\beta| \ . \tag{A12}$$

From Eq. (A3) it is obvious that the momenta $(\mathbf{p}_i,\mathbf{q}_i)$ form three dependent sets for the values $i=1,2,3$. The relations are linear and we can construct a 2×2 matrix α_{ji} such that

$$\begin{bmatrix} \mathbf{p}_j \\ \mathbf{q}_j \end{bmatrix} = \alpha_{ji} \begin{bmatrix} \mathbf{p}_i \\ \mathbf{q}_i \end{bmatrix} , \tag{A13}$$

with (ijk) cyclic. In case of the above choice of relative momenta we have

$$\alpha_{ji} = \begin{bmatrix} -\frac{1}{2} & +\frac{1}{2}\sqrt{3} \\ -\frac{1}{2}\sqrt{3} & -\frac{1}{2} \end{bmatrix} , \tag{A14}$$

with properties $\det\alpha = 1$, $(\alpha_{ji})^3 = \mathbf{I}$, $(\alpha_{ji})^{-1} = \alpha_{ij}$. The sets $(\mathbf{p}_j,\mathbf{q}_j)$ and $(\mathbf{p}_i,\mathbf{q}_i)$ are called mutually associated momenta.

Furthermore, we must concern ourselves with nucleonic spin and isospin degrees of freedom. At this level these quantum numbers are entirely independent, and complete quantum states are found by taking the direct product of spin and isospin states. Although the set of spin states $|s_1^z s_2^z s_3^z\rangle$ in Eq. (A1) forms a complete set, it is convenient to introduce orthonormal states

$$|(s_j s_k)s_p s_q; SS^z\rangle_i \ , \tag{A15}$$

where s_q is the spin of the spectator particle i and (ijk) again forms a cyclic order of (123). S and S^z denote the total spin and spin component of the three-nucleon state. The spins combine to $S=\frac{1}{2}$ (doublet) or $S=\frac{3}{2}$ (quartet). The spinnumber s_p arises from coupling the nucleon spins s_j and s_k. It either takes the value $s_p=0$ (singlet) or $s_p=1$ (triplet). The combination $s_p=0$, $S=\frac{3}{2}$ is excluded. Equation (A15) represents three spin states, if we ignore the magnetic spin component S^z. In an analysis with only s-wave NN interaction, this is a valid assumption and accordingly we introduce an abbreviated form of Eq. (A15)

$$|\chi_m^r\rangle_i \ , \tag{A16}$$

where r takes the values doublet or quartet and m takes the values singlet or triplet. Since the nucleonic spin and isospin are both $\frac{1}{2}$, treatment of these quantum numbers is entirely equivalent, and we introduce isospin basis states

$$|\eta_m^r\rangle_i \ , \tag{A17}$$

where the meaning of the labels is similar to Eq. (A16). To represent the spin-isospin states, we will often use the shorthand notation

$$|\beta\rangle_i = |(s_j s_k)s_p s_q SS^z;(t_j t_k)t_p t_q TT^z\rangle_i \ . \tag{A18}$$

The three-body analysis requires knowledge of the spin-isospin recoupling matrix elements ${}_j\langle\beta'|\beta\rangle_i$. In the recoupling, the total spin (isospin) is conserved. For the spin-doublet state we obtain with the aid of Edmonds' general recoupling coefficient[28]

$${}_j\langle\chi_{m'}^d|\chi_m^d\rangle_i = \begin{bmatrix} -\frac{1}{2} & +\frac{1}{2}\sqrt{3} \\ -\frac{1}{2}\sqrt{3} & -\frac{1}{2} \end{bmatrix} , \tag{A19}$$

where $m,m'=(s,t)$, and (ijk) is a fixed cyclic permutation of (123). To rule out any confusion, we explicitly state that in the chosen convention

$${}_2\langle\chi_t^d|\chi_s^d\rangle_1 = -\tfrac{1}{2}\sqrt{3} \ . \tag{A20}$$

The complete spin-isospin recoupling matrix restricted to pure doublet states therefore is

$$B_{ji} = {}_j\langle\chi^d|\chi^d\rangle_i \otimes {}_j\langle\eta^d|\eta^d\rangle_i = \begin{bmatrix} \frac{1}{4} & -\frac{3}{4} & \frac{1}{4}\sqrt{3} & -\frac{1}{4}\sqrt{3} \\ -\frac{3}{4} & \frac{1}{4} & \frac{1}{4}\sqrt{3} & -\frac{1}{4}\sqrt{3} \\ -\frac{1}{4}\sqrt{3} & -\frac{1}{4}\sqrt{3} & \frac{1}{4} & \frac{3}{4} \\ \frac{1}{4}\sqrt{3} & \frac{1}{4}\sqrt{3} & \frac{3}{4} & \frac{1}{4} \end{bmatrix} , \tag{A21}$$

where both the row and the column sequence of spin-isospin states is given by $\chi_t\eta_s,\chi_s\eta_t,\chi_s\eta_s,\chi_t\eta_t$. The matrix B_{ji} has the same properties as α_{ji}. The spin quartet recoupling is considerably simpler, since it involves only one channel

$${}_j\langle\chi_t^q|\chi_t^q\rangle_i = 1 \ . \tag{A22}$$

In the entire analysis we will regard particle 1 as the spectator particle, unless otherwise mentioned.

APPENDIX B: UPE DESCRIPTION OF s-WAVE LOCAL POTENTIAL

The homogeneous Lippmann-Schwinger (LS) equation for a central interaction,

$$\lambda_n g_n(p;s) = -4\pi\int_0^\infty dp' V(p,p')\frac{p'^2}{p'^2-s}g_n(p';s) \ , \tag{B1}$$

describes a physical bound state at $s=E_B<0$, if an eigenvalue $\lambda_n=1$ exists. In the UPE method the potential is

formally expanded in a complete set of eigenfunctions of the LS equation

$$V(p,p')=-\sum_{n=1}^{\infty}\lambda_n(s)g_n(p;s)g_n(p';s)\ . \tag{B2}$$

The UPA term corresponds to the first term of this series. The orthogonality relation,

$$4\pi\int_0^{\infty}dp\ g_m(p;s)\frac{p^2}{p^2-s}g_n(p;s)=\delta_{mn}\ , \tag{B3}$$

connects the Eqs. (B1) and (B2).

For the triplet channel the parameter s is fixed to the deuteron binding energy E_d, the value of which is about -2.228 MeV. The corresponding deuteron wave function coincides with the leading eigenfunction

$$\phi_d(\mathbf{p})=N_d\frac{1}{p^2-E_d}g_1(p;E_d)\ . \tag{B4}$$

The normalization constant N_d is determined according to

$$\int d\mathbf{p}|\phi_d|^2=1\ . \tag{B5}$$

To describe the virtual deuteron state one usually takes $s=0$ MeV,[22,23] which gives rise to a largest positive eigenvalue just below 1. But one can as well fix the singlet s value to the deuteron energy, which leads to a somewhat smaller largest eigenvalue. The major part of our results is calculated with the s value in both channels fixed to the deuteron energy E_d. In some situations we have studied the sensitivity of choosing the singlet s value equal to zero energy. It is explicitly mentioned in the text when this is done. Hereafter, we omit the notation of the parameter s.

For a separable potential, the two-body T matrix also takes a separable form. The partial wave components of the two-nucleon Lippmann-Schwinger T matrix are

$$t_l(p,p';\beta|z)=V_l(p,p';\beta)-4\pi\int_0^{\infty}dp''V_l(p,p'';\beta)\times\frac{p''^2}{p''^2-z}t_l(p'',p';\beta|z)\ , \tag{B6}$$

where

$$t(\mathbf{pp}';\beta|z)=\sum_{l=0}(2l+1)P_l(\hat{\mathbf{p}}\cdot\hat{\mathbf{p}}')t_l(p,p';\beta|z)\ . \tag{B7}$$

In UPE the s-wave T matrix can be written as

$$t(p,p';\beta|z)=\sum_{jk}g_j(p;\beta)\tau_{jk}(z;\beta)g_k(p';\beta)\ , \tag{B8}$$

where we have omitted the partial wave label. The propagator τ_{jk} can be directly obtained from matrix inversion

$$\tau_{jk}(z;\beta)=-\left[\lambda_j^{-1}\delta_{jk}-4\pi\int_0^{\infty}dp\,p^2\frac{g_j(p;\beta)g_k(p;\beta)}{p^2-z}\right]^{-1}\ . \tag{B9}$$

Also in the continuum region the UPE T matrix is unitary for any number of terms. This property is due to the fact that the expansion of the potential is symmetric and real in each term. Furthermore, fixing s to E_d implies that the UPA T matrix already contains the entire local T matrix around the deuteron point; increasing the number of terms does not affect its position.

APPENDIX C: THE FADDEEV EQUATIONS

The construction of the half-off-shell $NNN\rightarrow Nd$ scattering wave function requires the solution of the Faddeev equations. Assuming a sum of pairwise potentials,

$$V=V_1+V_2+V_3\ .$$

and decomposing the three-particle Lippmann-Schwinger T matrix as

$$T(z)=T^1(z)+T^2(z)+T^3(z)\ , \tag{C1}$$

the Faddeev equations can formally be written as

$$T^k(z)=t_k(z)-t_k(z)G_0(z)\sum_{m\neq k}T^m(z)\ , \tag{C2}$$

where t_k denotes the two-nucleon T matrix acting in pair k. The resolvent operator $G_0(z)$ is taken as

$$G_0(z)=(H_0-z)^{-1}\ . \tag{C3}$$

It is useful to introduce a more extended decomposition of the T matrix,

$$T_l^k(z)=t_k(z)\delta_{kl}-t_k(z)G_0(z)\sum_{m\neq k}T_l^m(z) \tag{C4}$$

with the obvious property

$$\sum_l T_l^k(z)=T^k(z)\ . \tag{C5}$$

For example, the rearrangement scattering amplitude is determined by

$$M_{\text{rearr}}=\frac{1}{2}\sum_m {}_j^A\langle\alpha_f\mathbf{q}_f\beta_f|U_{jm}|\alpha_i\mathbf{q}_i\beta_i\rangle_m^A\ , \tag{C6}$$

where the transition operator U_{jk} can be constructed from the T_l^k matrix elements according to

$$U_{\alpha\beta}(z)=\sum_k V_k(1-\delta_{k\alpha})\delta_{k\beta}+\sum_{\substack{k\neq\alpha\\ l\neq\beta}}T_l^k(z)\ . \tag{C7}$$

The label A in Eq. (C6) indicates that the initial and final state are antisymmetrized in the pair denoted by the subindex; the factor $\frac{1}{2}$ is due to the normalization of the state $|\alpha\mathbf{q}\beta\rangle^A$.

Apart from the Born contributions, the electromagnetic two-body breakup amplitude is proportional to

$${}_1^A\langle\mathbf{p}_1\mathbf{q}_1\beta_1|\sum_{\substack{klm\\ l\neq m\\ k\neq 1}}T_l^k(z)|\alpha_f\mathbf{q}_f\beta_f\rangle_m^A\ . \tag{C8}$$

Inserting a complete set of basis states [Eq. (A12)] leads to the equivalent expression

$$\frac{1}{2}\sum_{\beta}\int dp\,dq\,{}_1^A\langle \mathbf{p}_1\mathbf{q}_1\beta_1|\mathbf{pq}\beta\rangle_2^A \times \sum_{\substack{klm\\ l\neq m\\ k\neq 1}} {}_k^A\langle \mathbf{pq}\beta|t_l^k(z)|\alpha_f\mathbf{q}_f\beta_f\rangle_m^A , \quad \text{(C9)}$$

where we have used a property due to the identity of particles

$${}_i^A\langle \mathbf{p}_1\mathbf{q}_1\beta_1|\mathbf{pq}\beta\rangle_j^A = {}_i^A\langle \mathbf{p}_1\mathbf{q}_1\beta_1|\mathbf{pq}\beta\rangle_k^A \qquad i\neq j\neq k\neq i . \quad \text{(C10)}$$

Following Kloet[13] we introduce the half-off-shell function

$$U(\mathbf{p},\mathbf{q};\beta)=\frac{1}{2}\sum_{\substack{klm\\ l\neq m\\ k\neq 1}} {}_k^A\langle \mathbf{pq}\beta|T_l^k(z)|\alpha_f\mathbf{q}_f\beta_f\rangle_m^A , \quad \text{(C11)}$$

Applying Eq. (C4) and inserting a complete set once more, we find that U satisfies the integral equation

$$U(\mathbf{p},\mathbf{q};\beta)=2\,{}_2^A\langle \mathbf{pq}\beta|t_2(z)|\alpha_f\mathbf{q}_f\beta_f\rangle_1^A - \sum_{\beta'}\int dp'dq'\frac{1}{p'^2+q'^2-z} \times {}_2^A\langle \mathbf{pq}\beta|t_2(z)|\mathbf{p}'\mathbf{q}'\beta'\rangle_1^A \times U(\mathbf{p}',\mathbf{q}';\beta') , \quad \text{(C12)}$$

where in addition to Eq. (C10) use has been made of the permutation property

$$P_i t_j(z) P_i = t_k(z), \quad i\neq j\neq k\neq i . \quad \text{(C13)}$$

The integral equation for U in Eq. (C12) is derived without making any restrictions or assumptions. The solution of U enables us to determine the most general off-shell scattering amplitude with an initial or final *Nd* state. However, in practice we need to truncate Eq. (C12) to a limited number of channels. First we restrict the *NN* interaction to only the *s*-wave channels. This implies that in the active subsystem the angular momentum number $l_p=0$. From the parity requirement stated in Eq. (A11) we see that the remaining subsystem quantum numbers $\beta_p=s_p+t_p$ must be odd. This reduces Eq. (C12) to two sets of two-dimensional integral equations for each partial wave number of the spectator momentum $\mathbf{q}$. A coupled set for the spin-isospin channels $\chi_t^d\eta_s^d$ and $\chi_s^d\eta_t^d$ and an uncoupled set for the spin quartet channel $\chi_t^q\eta_s^d$. Scattering in the $\chi_s^d\eta_t^q$ channel is avoided due to the isospin-singlet nature of the deuteron.

The derivation of the *Nd* scattering equation for an *s*-wave local interaction has been presented and discussed in full detail by Kloet.[13] In the subsequent analysis the local potential is replaced by its unitary pole approximation. Use of a separable potential has the clear advantage that the integral equations become one dimensional, which will certainly speed up the numerical evaluations.

TABLE V. Three-nucleon (iso)spin coefficients for the break-up analysis.

	χ_s^d	$\sigma^z_{(1)}$ χ_t^d	χ_t^q	χ_s^d	$\sigma^z_{(\pm)}$ χ_t^d	χ_t^q
χ_s^d	±1	0	0	0	$\mp\frac{1}{\sqrt{3}}$	$\sqrt{2/3}$
χ_t^d		$\mp\frac{1}{3}$	$-\frac{2}{3}\sqrt{2}$		$\pm\frac{2}{3}$	$\frac{1}{3}\sqrt{2}$
χ_t^q			$\pm\frac{1}{3}$			$\pm\frac{1}{3}$

From the on-shell *Nd* scattering amplitude the phase parameters η and δ can be obtained, using amplitude[32] according to

$$M_l^S=-\left[\frac{dE(q)/dq}{\pi q^2}\right]\frac{^{2S+1}\eta_l\exp(2i\,{}^{2S+1}\delta_l)-1}{2i} , \quad \text{(C14)}$$

where l and S label the spectator partial wave number and the trinucleon spin channel in which the scattering takes place. The amplitude M_l^S results from a partial wave decomposition of the complete scattering amplitude expressed in Eq. (C6). The spectator momentum q is, of course, related to the energy through

$$q^2=q_i^2=q_f^2=T_{Nd} . \quad \text{(C15)}$$

For completeness we give the explicit expressions for the phase shift and the inelasticity

$$\tan\delta=\frac{\mathrm{Im}M_l^S}{\mathrm{Re}M_l^S}-\frac{\eta-1}{(\pi q)\mathrm{Re}M_l^S} , \quad \text{(C16)}$$

$$\eta=[(\pi q)^2|M_l^S|^2+2\pi q\,\mathrm{Im}M_l^S+1]^{1/2} , \quad \text{(C17)}$$

where $\eta\leq 1$ due to unitarity.

APPENDIX D: SPIN-ISOSPIN COEFFICIENTS

The quantities S_μ^λ expressed in Eq. (68) still contain the spin matrix elements ${}_1\langle\chi^{(i)}|\sigma_{(n)}|\chi^{(f)}\rangle_1$. In the pure *s*-wave analysis it is sufficient to know the spin elements for the z component. Table V lists all relevant numbers. The left-hand side applies to $n=1$, the right-hand side to odd or even combinations of $n=2,3$ according to Eq. (75). In $s\to s$, $t\to t$ transitions we need the $\sigma^z_{(+)}$ term, whereas the $\sigma^z_{(-)}$ term is only relevant in the $s\leftrightarrow t$ flip transitions. Some numbers in the table are double signed. The upper sign corresponds to the three-nucleon spin component $S^z=+\frac{1}{2}$, the lower sign to $S^z=-\frac{1}{2}$. (The quartet-quartet coefficient for $S^z=\pm\frac{3}{2}$ is ±1 for both $\sigma^z_{(1)}$ and $\sigma^z_{(+)}$.) Since the treatment of spin and isospin is completely equivalent, Table V can also serve to determine the isospin elements ${}_1\langle\eta^{(i)}|\tau^z_{(n)}|\eta^{(f)}\rangle_1$. Simply replace S by T, σ by τ, and χ by η in the above description and the corresponding table.

[1]S. Frullani and J. Mougey, Adv. Nucl. Phys. **14**, 1 (1984).
[2]E. Jans *et al.*, Phys. Rev. Lett. **49**, 974 (1982).
[3]E. Jans *et al.*, Nucl. Phys. **A475**, 687 (1987).
[4]P. H. M. Keizer, P. C. Dunn, J. W. A. den Herder, E. Jans, A. Kaarsgaarn, L. Lapikás, E. N. M. Quint, P. K. A. de Witt Huberts, H. Postma, and J. M. Laget, Phys. Lett. **157B**, 255 (1985).
[5]P. H. M. Keizer, J. F. J. van den Brand, J. W. A. den Herder,

E. Jans, L. Lapikás, E. N. M. Quint, P. K. A. de Witt Huberts, and H. Postma, Phys. Lett. B **197**, 29 (1987).
[6]H. Meier-Hajduk, C. H. Hajduk, P. U. Sauer, and W. Theis, Nucl. Phys. **A395**, 332 (1983).
[7]C. Ciofi degli Atti, E. Pace, and G. Salmè, Phys. Lett. **127B**, 303 (1983).
[8]J. M. Laget, Phys. Lett. **151B**, 325 (1985), and private communication.
[9]J. M. Laget, Phys. Lett. B **199**, 493 (1987).
[10]I. M. Barbour and A. C. Philips, Phys. Rev. C **1**, 165 (1970).
[11]D. R. Lehman, Phys. Rev. C **3**, 1827 (1971); C. R. Heimbach, D. R. Lehman, and J. S. O'Connell, Phys. Lett. **66B**, 1 (1977); B. F. Gibson and D. R. Lehman, Phys. Rev. C **29**, 1017 (1984).
[12]R. A. Malfliet and J. A. Tjon, Nucl. Phys. **A127**, 161 (1969); Ann. Phys. **61**, 425 (1970).
[13]W. M. Kloet and J. A. Tjon, Ann. Phys. (N.Y.) **79**, 407 (1973).
[14]T. de Forest, Jr., Nucl. Phys. **A392**, 232 (1983).
[15]S. Boffi, C. Giusti, and F. D. Pacati, Nucl. Phys. **A386**, 232 (1983).
[16]G. Höhler, E. Pietarinen, I. Sabba-Stefanescu, F. Borkowski, G. G. Simon, V. H. Walther, and R. D. Wendling, Nucl. Phys. **B114**, 505 (1976).
[17]A. M. Bincer, Phys. Rev. **118**, 855 (1960).
[18]H. L. W. Naus and J. H. Koch, Phys. Rev. C **36**, 2459 (1987).
[19]H. L. W. Naus, S. J. Pollock, and J. H. Koch (unpublished).
[20]A. E. L. Dieperink, T. de Forest, Jr., I. Sick, and R. A. Brandenburg, Phys. Lett. **63B**, 261 (1976).
[21]J. Mougey, M. Bernheim, A. Bussière, A. Gillebert, Phan Xuan Hô, M. Priou, D. Royer, I. Sick, and G. J. Wagner, Nucl. Phys. **A262**, 461 (1976).
[22]E. Harms, Phys. Rev. C **1**, 1667 (1970); E. Harms and V. Newton, *ibid.* **2**, 1214 (1970).
[23]B. L. G. Bakker and P. Ruig, in *Proceedings of the International Conference on Few Particle Problems in the Nuclear Interaction, Los Angeles, 1972,* edited by I. Slaus, S. A. Moszkowski, R. P. Haddock, and W. T. H. van Oers (North-Holland, Amsterdam, 1973), p. 357.
[24]J. A. Tjon, Phys. Rev. D **1**, 2109 (1970).
[25]G. L. Payne, J. L. Friar, B. F. Gibson, and I. R. Afnan, Phys. Rev. C **22**, 823 (1980).
[26]D. H. E. Gross and R. Lipperheide, Nucl. Phys. **A150**, 449 (1970).
[27]E. van Meijgaard and J. A. Tjon (unpublished).
[28]A. R. Edmonds, *Angular Momentum in Quantum Mechanics* (Princeton University Press, Princeton, NJ, 1957).
[29]K. L. Kowalski, Phys. Rev. Lett. **15**, 798 (1965); H. P. Noyes, *ibid.* **15**, 538 (1965).
[30]A. Johansson, Phys. Rev. **136**, B1030 (1964).
[31]B. F. Gibson and G. B. West, Nucl. Phys. **B1**, 349 (1967).
[32]M. L. Goldberger and K. M. Watson, *Collision Theory* (Wiley, New York, 1964).

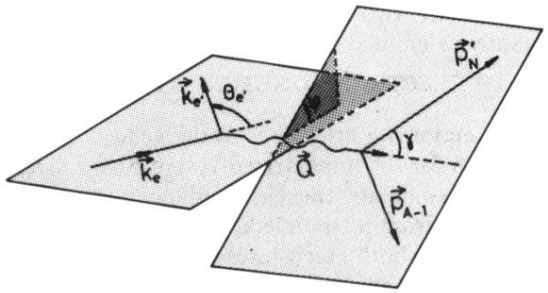

FIG. 2. Kinematic structure of $(e,e'p)$ reaction.